



A Review of Modern Assessment Methods for Metal and Metal-Oxide Based Primers for Substrate Corrosion Protection

Matthew E. McMahon*, Raymond J. Santucci Jr., Carol F. Glover, Balaji Kannan, Zachery R. Walsh and John R. Scully

Department of Materials Science and Engineering, Center for Electrochemical Science and Engineering, University of Virginia, Charlottesville, VA, United States

OPEN ACCESS

Edited by:

Flavio Defforian,
University of Trento, Italy

Reviewed by:

Guido Grundmeier,
University of Paderborn, Germany
Ricardo M. Souto,
Universidad de La Laguna, Spain
Fatima Montemor,
Higher Technical Institute, University of
Lisbon, Portugal

*Correspondence:

Matthew E. McMahon
mm5kn@virginia.edu

Specialty section:

This article was submitted to
Environmental Materials,
a section of the journal
Frontiers in Materials

Received: 26 April 2019

Accepted: 24 July 2019

Published: 06 September 2019

Citation:

McMahon ME, Santucci RJ Jr, Glover CF, Kannan B, Walsh ZR and Scully JR (2019) A Review of Modern Assessment Methods for Metal and Metal-Oxide Based Primers for Substrate Corrosion Protection. *Front. Mater.* 6:190.
doi: 10.3389/fmats.2019.00190

Pigmented coatings developed for the corrosion protection of engineering alloys have been successful in the field of corrosion control, and thus are ubiquitous in application. Supporting this success are an array of methods to diagnostically assess these systems and measure their state of degradation. These methods assist the development of next generation coatings, in-service evaluation, and post-mortem analysis of performance. This review comprehensively explores these modern assessment methods, used to screen candidate corrosion prevention pigments, assess pigment protection efficiency, quantify overall pigment effectiveness, and/or predict coating service lifetime. Coating service life assessment is conducted based on the class of coating considered, as categorized by (1) chemical inhibition, (2) galvanic protection, (3) high impedance ion barrier, or a combination of these protection mechanisms. Exciting new *in-situ* and operando methods are growing in use to enable high fidelity measurement of chemical inhibitor release and deposition, such as micro and *in-situ* Raman spectroscopy and inductively coupled plasma atomic emission spectrometry (ICP-AES), to name a few. In the galvanic protection coating class, service life and the state of coating performance are now being quantified through methods such as galvanostatic pulse and accelerated cycle testing. Galvanic throwing power is assessed by scanning vibrating electrode technique (SVET), multi-electrode array (MEA), and scanning kelvin probe (SKP). The performance of high impedance ion barrier coatings has traditionally been understood through use of electrochemical impedance spectroscopy (EIS) and equivalent circuit modeling, which have been applied to all coating classes. Finite element analysis (FEA) models the combined effects of coating resistance, water layer thickness, and pigment potential on galvanic coupling and/or inhibitor species release as well. The development of effective corrosion prevention pigments and the in-service evaluation of their efficiency/effectiveness demands a broad collection of techniques. These methods now include new advances in thermodynamic modeling via chemical stability diagrams to

assess pigment function in specific conditions, *in-situ* pH measurement, as well as energy dispersive (EDS) and x-ray photoelectron spectroscopic (XPS) analyses to determine elemental distribution and corrosion product formation. These techniques and more are explored in this review to document the state-of-the-art in the field.

Keywords: metal-rich primers, zinc, magnesium, chemical inhibition, SVET, chemical stability modeling

INTRODUCTION

The cost of corrosion was estimated to be 3–4% of each nation's gross national product (GDP) in 2013, or a global cost of approximately US\$2.5 trillion per year (Koch, 2017). The global use of effective corrosion control practices (protective coatings, considerate design strategies, regular preventative maintenance, etc.) is estimated to reduce this cost by 15–35%, or as much as US\$875 billion annually (Koch, 2017). One means of achieving this savings is through the effective design and application of protective coatings such as metal-rich primers, which are now ubiquitous across many engineering sectors to prevent corrosion and extend service life. Metallic corrosion requires thermodynamically viable anodic and cathodic reactions, as well as electrical and ionic conduction between anodes and cathodes. Pigmented coatings such as metal-rich primers, which are composed of sacrificial pigments embedded within an adhesive resin, operate through a variety of means, such as chemical inhibition, galvanic protection, and high impedance barrier protection. These coatings can be designed to alter the dominant anodic/cathodic reactions that occur, limit one or more of the corrosion cell requirements, or even to introduce a new sacrificial anodic reaction to afford corrosion protection to the substrate. The means of protection is dependent upon the type of sacrificial pigment present, the connectivity of the pigment, and the resin type/porosity, to name a few factors. These coatings do not necessarily function in exactly the same manner as metallic coatings, which are thin metal/alloy layers often electro- or vapor-deposited on an alloy surface, where the entirety of the layer is barrier and/or sacrificial and no binding resin is present. The same sacrificial metals may be utilized in both coating types, though the metal-rich primer design offers certain benefits, such as the ability to delay primer activation through the resin or topcoat and reduce the self-corrosion rate by isolating a portion of the particles, as well as the versatile ability to be spray-coated on nearly any free surface (though proper adhesion can be elusive). A key aspect of metal-rich primer (MRP) performance is the ability of the primer to protect latent or operational defects such as scratches as well as the substrate under the intact coating. Effective design of metal-rich primers to achieve such performance requires specific tuning for each chosen alloy substrate, and this tuning is informed by a variety of characterization methods (Bierwagen et al., 2007; Yan et al., 2010; King and Scully, 2011; King et al., 2014a, 2015; Bastos et al., 2016; Santucci et al., 2017a, 2018a).

Through purposeful MRP design, the influence of these coatings may substantially improve long-term component integrity and survivability. On near-shore gas pipelines (steel),

for example, inorganic Zn-rich primers have been observed to maintain corrosion protection for over 50 years (Francis, 2013); on offshore steel platforms, similar primers have been demonstrated to delay the onset of red rust for 10 years or more (Feliu et al., 2001). Thus, Zn-rich primers have become especially useful for steel protection. Zn-based primers (ZnRPs) function mainly through galvanic interactions with the substrate to provide sacrificial protection, and with time of exposure the buildup of corrosion products has been demonstrated to offer secondary impedance barrier protection and/or chemical protection as well (Feliu et al., 1993a,b, 2001; Bierwagen et al., 2007; Hammouda et al., 2011; Krieg et al., 2012; Cubides and Castaneda, 2016; McMahon et al., 2019a). Magnesium-based MRPs (MgRPs) have been demonstrated to continue providing substrate protection on aluminum after 4 years' atmospheric exposure even after all sacrificial metallic pigment has been converted to MgO through a combined galvanic and chemical inhibition mechanism (Santucci et al., 2017a,b). The specific mechanisms through which MgRPs operate are not fully understood. Research findings demonstrate synergistic impacts through several chemical mechanisms (i.e., pH buffering upon Mg^{2+} diffusion to the exposed substrate as well as MgO formation, which has been supported through tests on MgO-rich primers) (Santucci et al., 2017a,b, 2018a), galvanic mechanisms (the galvanic couple potential achieved as Mg pigment volume concentration (PVC) is adjusted) (King and Scully, 2011; King et al., 2014a, 2015), as well as possible coating and corrosion product secondary impedance effects (Nanna and Bierwagen, 2004; Krieg et al., 2012; Stoulil et al., 2015). Of course, MRPs may also cause rather than delay substrate degradation if not properly designed. The interactions between MRPs, the surrounding environment, and macro-defects exposing the substrate are complex, as are the specific combinations of mechanisms through which these coatings operate in unique scenarios. For example, ZnRPs on one high strength armor steel accelerated corrosion and hydrogen embrittlement due to the achievement of overly cathodic potentials (severely hydrogen-generating) (Koul et al., 2014), whereas on a pipeline steel similar ZnRPs suppressed corrosion for decades (Francis, 2013). Thus, well-informed and purposeful design of MRP technologies is necessary to maximize the corrosion protection, subsequent reliability, and cost savings possible through use of MRPs. This is possible through thorough MRP testing and performance evaluation in pertinent environmental conditions.

The wide variety of MRP types, functions, and characterization methods will be reviewed herein to inform further design optimization of these corrosion prevention systems. This review will first discuss the modes of MRP

protection, their specific attributes, and the known primer characteristics that may lead to a given type of performance. A key consideration will be mechanisms for “active corrosion inhibition” of a meso- or macro-defect exposing the bare substrate. Following this baseline, the means of characterizing each type of MRP will be reviewed, which will lead into a brief discussion on the future of MRP-based corrosion prevention as well as primer development.

METAL-RICH PRIMER PERFORMANCE ATTRIBUTES

Chemical Inhibition

Metal-rich primers may achieve corrosion prevention via the storage and release of corrosion inhibiting agents, which suppress anodic/cathodic reactions at macro-defects and possibly under the coatings. These inhibitors are often situated in three ways: (1) global deployment of the inhibitor into the solution which comes into contact with the substrate, as with gas/oil/drinking water pipelines, reactors, rinses, etc.; (2) direct application to the substrate either in a conversion coating or a metallic coating; and (3) incorporation into a composite coating where the inhibitor is embedded, such as in a particle, within an organic or inorganic polymer matrix, as with MRPs (Gharbi et al., 2018). These deployment methods and their functions are schematically summarized in **Figure 1** (Gharbi et al., 2018). This review will be primarily concerned with type (3), wherein the chemical inhibitor comprises or is part of the sacrificial particles embedded within a resin, though techniques and strategies for assessment may be applicable throughout.

Inhibitor protection is considered an “active protection mode” where inhibitor species can be released from intact portions of coating to chemically protect the exposed substrate after barrier protection has been compromised (Xia et al., 2000; Presuel-Moreno et al., 2005a, 2006, 2008; Ho et al., 2006). The presence of the resin places increased importance on the selective release of inhibitors, which will affect the sensitivity and the service life of these primers. A smart coating is the most desirable because such systems are triggered to selectively release chemical inhibitors by specific changes in pH, O₂ content, ultraviolet light, certain established potentials, and more (Zheludkevich et al., 2012; Montemor, 2014), as demonstrated in **Figure 1**. In this way, the coating may exhibit delayed and purposeful activation only in response to conditions that would otherwise promote corrosion events. In the Al-Co-Ce system, for example, release rates of Co- and Ce-based inhibitors depend on pH and [Cl⁻] (Jakab and Scully, 2008). The release of chromate from chromate conversion coatings has also been demonstrated to occur as a function of pH and ionic strength (Xia et al., 2000). In general, the dissolution process is driven by thermodynamics, or the free energy change achieved by the dissolution of the solid phase inhibitor package into aqueous phase inhibitor species and by-product species. **Figure 2** demonstrates how the driving force for dissolution is dependent on the subsequent change in free energy, which is related to the concentration of species produced according to Equation 1, where Q is the reaction quotient and K_{SP}

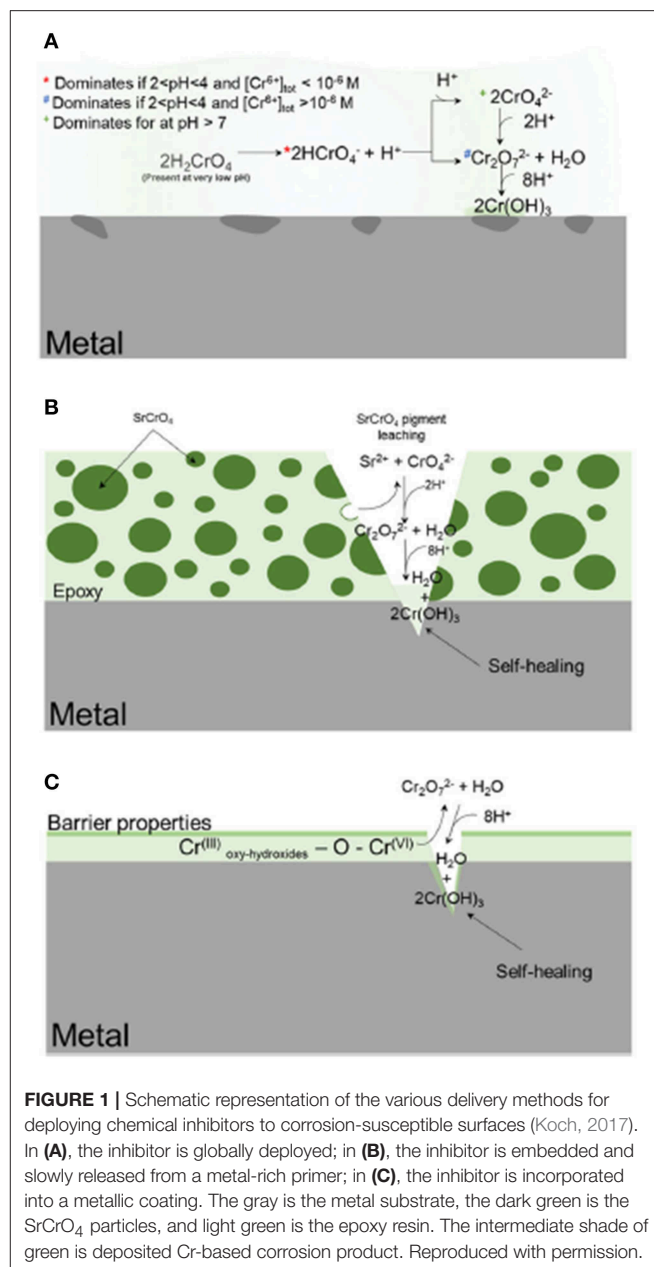
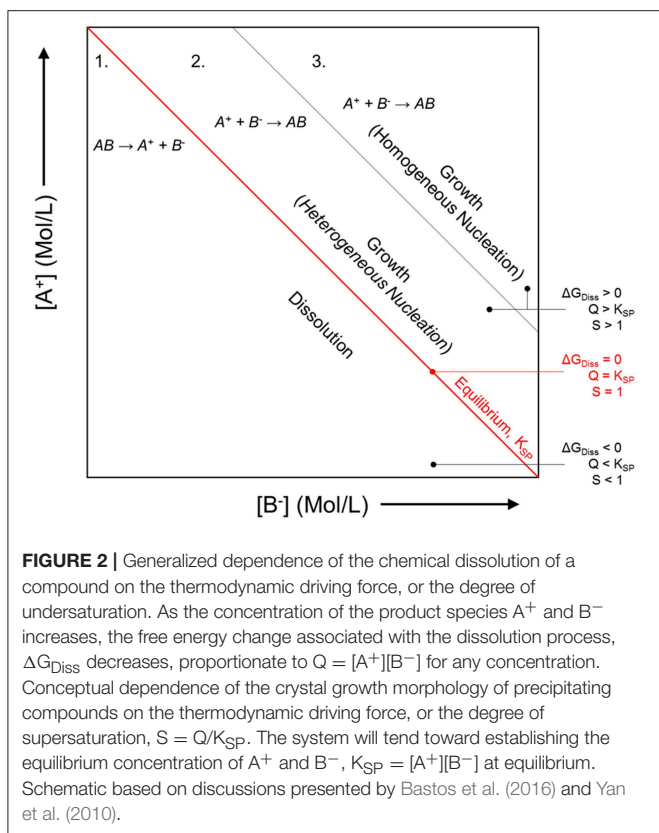


FIGURE 1 | Schematic representation of the various delivery methods for deploying chemical inhibitors to corrosion-susceptible surfaces (Koch, 2017). In **(A)**, the inhibitor is globally deployed; in **(B)**, the inhibitor is embedded and slowly released from a metal-rich primer; in **(C)**, the inhibitor is incorporated into a metallic coating. The gray is the metal substrate, the dark green is the SrCrO₄ particles, and light green is the epoxy resin. The intermediate shade of green is deposited Cr-based corrosion product. Reproduced with permission.

is the equilibrium solubility product. There is a decrease in the free energy of the system caused by dissolution when $Q < K_{SP}$. An alternative metric which is sometimes used is the saturation index, S, defined as simply the ratio of Q to K_{SP} (Barker et al., 2018). Similarly, when $S < 1$, dissolution is favorable. When $S > 1$, dissolution is not favorable, and precipitation is likely to occur. When $Q = K_{SP}$, $\Delta G = 0$, $S = 1$, and the system is in equilibrium:

$$\Delta G_{Diss} = RT \ln \left(\frac{Q}{K_{SP}} \right)$$

Dissolution processes are often activation-controlled in rate (Frankel et al., 2018). This means that the rate is proportionate



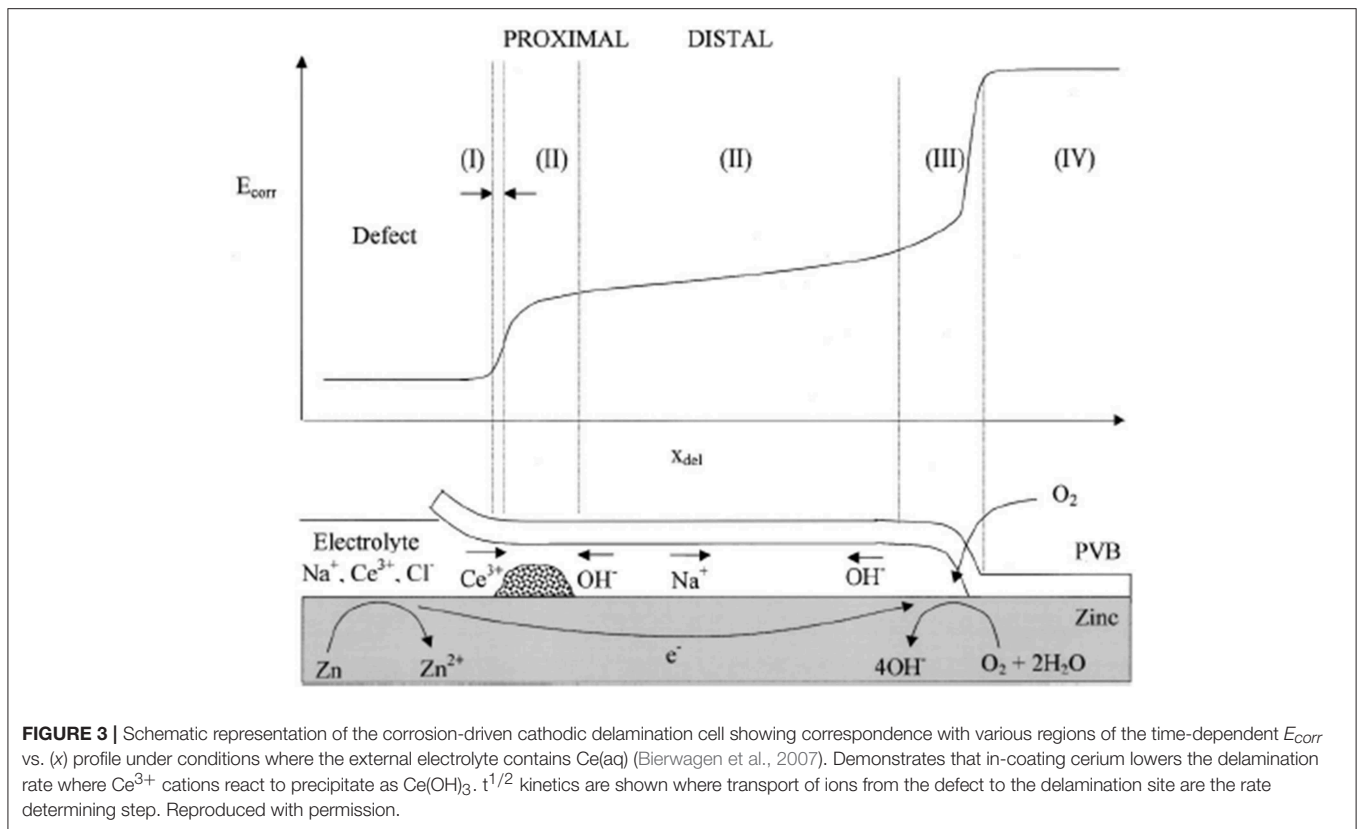
to the thermodynamic driving force. For chemical dissolution processes, this is often described by the Transition State Theory (Frankel et al., 2018). For electrochemical processes, activation-controlled dissolution regulated at the metal-electrolyte interface is described by the Butler-Volmer equation (Frankel et al., 2018). Butler-Volmer kinetics may be utilized to describe the dependency of electrochemical dissolution rates on the chemical inhibitor particle, because these interfacially-controlled processes occur in proportion to the thermodynamic driving force that is present (Hellmann and Tisserand, 2006; Frankel et al., 2018). Since electrons participate in electrochemical reactions as a reacting species, the total rate of dissolution is dependent upon the electrode potential. Other processes can control the interfacial dissolution of inhibitor packages, such as mass transport limitations or the formation of some rate-limiting interfacial film (Frankel et al., 2018).

The transport of the inhibitor from the inhibitor package to the corrosion site is the next critical aspect of the chemical inhibition performance, which can be driven by diffusion/migration (based on activity or potential differences), convection, and other processes. Migration of the Ce^{3+} inhibitor has been successfully modeled to explain the transport of these species into a coating defect, such as a scribe (Akiyama et al., 2003; Presuel-Moreno et al., 2006). Once in contact with the substrate, the inhibitor may affect electrochemical processes in a variety of ways, including but not limited to affecting the charge transfer necessary for important anodic or cathodic reactions,

promoting passive film growth with semiconductive properties, or forming physical diffusion barriers. Numerous works have demonstrated that chemical inhibitors tend to precipitate solid films on the substrate, which may occur chemically (Aldykewicz et al., 1995; Williams et al., 2002; Presuel-Moreno et al., 2005b) or electrochemically (Xia et al., 2000; Presuel-Moreno et al., 2005b). In these cases, the site specificity and morphology of the precipitated films must be understood, which will depend on the thermodynamic driving forces (Figure 2; Lasaga, 2014). The thermodynamic formation conditions for such surface films formed through precipitation and scaling processes may be understood through chemical stability diagram predictions, which will be discussed in an ensuing section.

Inhibitor protection is promoted by high storage capacity in the coating, low threshold concentrations for inhibitor efficacy [$c_{i(\text{crt})}$], and controlled inhibitor release based on intermediate solubility whereby the inhibitor concentration is delivered within a solubility window at which the inhibitor concentration is above $c_{i(\text{crt})}$ but below some high threshold concentration for osmotic blistering (Sinko, 2001). The efficacy of chemical inhibitors is based on the affinity of the inhibitor to affect the rate-limiting anodic or cathodic reactions occurring on the substrate. Thus, the proper selection of chemical inhibitor for storage in a pigment requires that the controlling reaction process be understood for the specific alloy in need of protection. On AA2024-T351, ultramicroelectrode array analysis demonstrated that oxygen reduction reaction (ORR) kinetics occurring on Cu-rich sites were limited either by surface coverage due to Cu replating or the diffusional boundary layer thickness (Presuel-Moreno et al., 2005a). In this well-studied alloy system, the inhibiting species Ce^{3+} , Co^{3+} , and MoO_4^{2-} were evaluated, all of which were shown to affect the cathodic reaction through different means (blocking Cu-rich sites, forming a surface film, etc.) (Scully and Jakab, 2006). Specifically, these inhibitors have been demonstrated to reduce the cathodic kinetics of ORR on pure Cu (Aldykewicz et al., 1995; Presuel-Moreno et al., 2005b; Yasakau et al., 2006). Ce^{3+} and La^{3+} ions have also been demonstrated to act as anodic reaction inhibitors elsewhere (Kaesche, 1985; Aldykewicz et al., 1995; Frankel and McCreery, 2001; Ilevbare and Scully, 2001; Yasakau et al., 2006).

The effect of such ions has been explored using a scanning kelvin probe (SKP) to investigate their effect on under-film cathodic delamination at a defect (Williams et al., 2002). The study of cathodic delamination using SKP was pioneered by Stratmann and the technique is now well-utilized for the assessment of the corrosion protection afforded by organic coatings (Stratmann et al., 1994; Rebhan et al., 2003). This technique has also proven useful to screen inhibitor-containing conductive polymer coatings for their ability to minimize corrosion on the buried metal-coating interface (Rohwerder et al., 2009, 2011). Scanning kelvin probe is a completely non-perturbing technique and allows the temporal and spatial resolution of potential distributions beneath intact organic coatings. This method has been employed in previous studies to gain mechanistic understanding of the delamination corrosion cell on important metal substrates (Williams and McMurray, 2001; Williams et al., 2002). A gold probe, which has an



electrical connection with the specimen via an external circuit, is rastered above the specimen surface at a height of approx. $100\ \mu\text{m}$. The potential required to null the resultant current flow between probe and specimen is measured. This is the Volta potential difference, which can be converted to corrosion potential (E_{corr}) via application of a conversion factor (Leng et al., 1998; Grundmeier et al., 2000; Williams and McMurray, 2001). Experiments are conducted inside a Faraday cage that also enables control of the humidity, which must be maintained at a consistently high level. In the experiments designed by Stratmann, electrolyte is placed in a large macro-defect created in the polymer. The progression of a cathodic delamination front can then be monitored by profiling the area in the vicinity of the defect with the vibrating gold probe (Figure 3). A full description of the experimental set up can be found elsewhere (Stratmann et al., 1994; Rebhan et al., 2003).

Galvanic Protection

Galvanic protection mechanisms differ from chemical inhibition mechanisms due mostly to the need for galvanic coupling between the sacrificial anodic particles and the substrate, rather than self-corrosion of the particles in response to the surrounding chemistry. In conditions where galvanic coupling is maintained, the overarching goal is to maintain coupled potentials below some critical threshold, such as the substrate breakdown potential (cathodic prevention) (McMahon et al., 2019a), or at a selected magnitude of overpotential to reduce corrosion reaction rates (cathodic protection) (Feliu et al., 2001). These terms, as

well as others which are critical to this review, are defined further in Table 1. According to mixed potential theory, the quantity of exposed sacrificial particles connected to the substrate will affect the coupled potential and the overall corrosion rate in the substrate. This galvanic couple is mediated by the electron transfer kinetics of the anodic pigment, the cathodic substrate, and also the electrical/ionic resistance between the two. The optimal pigment choice requires a specific balance consisting of the achievement of necessary coupled potentials below the open circuit potential (OCP) of the substrate, enduring activity of the pigment to resist passivation/coating deactivation, and fast sacrificial anodic kinetics. Purposeful alloying can assist in reaching this balance, as has been achieved in Mg-based systems for various modes of corrosion protection (Plagemann et al., 2013; Glover et al., 2019).

Cathodic protection is promoted by low coating matrix resistivity, fast pigment anodic kinetics, low pigment corrosion potential, high pigment loading, and low coating polarizability. Increasing the PVC is known to directly impact these performance attributes, since the particle packing dictates the amount of connectivity between the particles to sustain high anodic charge output. This effect has been demonstrated in MgRPs having an epoxy resin on AA2024 up to the critical PVC (CPVC) of 65% (Figure 4; King and Scully, 2011). In ZnRPs, the use of lamellar Zn particles has been demonstrated to be effective in galvanic protection up to 40% CPVC, and when using spherical Zn particles this value increased to 65% CPVC (Kalendová, 2003; Shreepathi et al., 2010). The PVC correlates

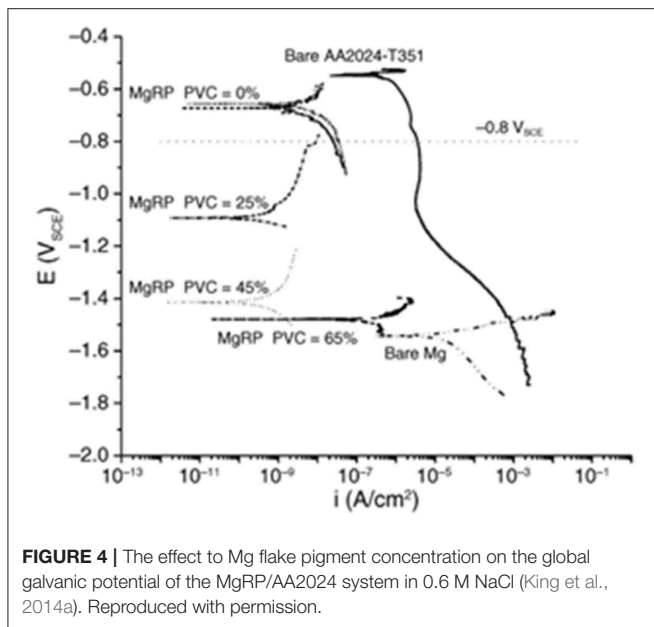
TABLE 1 | Glossary of critical terms for the topic of metal-rich primers.

Glossary of terms	
Coating	A layer of material fabricated on the surface of a substrate to provide protection by physical, electrochemical, and/or chemical means.
Conversion coating	A type of coating formed on the surface of a metal via a chemical or electrochemical process to provide corrosion protection. There are three types of common conversion coatings: oxide, phosphate, and chromate. Conversion coatings may be a portion of an overall coating system which may also include a primer and topcoat.
Cathodic protection	A corrosion protection mechanism in which a galvanic couple is used to reduce corrosion rates of the protected substrate according to the magnitude of potential difference between the applied potential and the floating open circuit potential of the substrate.
Cathodic prevention	A corrosion protection mechanism in which potential is maintained below a critical potential such as the breakdown potential above which a passive film formed on the substrate will deteriorate.
Defect	With respect to a coating, a defect is a portion of the coating in which barrier protection has been compromised, and active protection schemes are required. Examples and various names for defects include, but are not limited to: scratch, scribe, scribe creep, delamination, crack, pore, holiday, pin-hole, blister, and void. Defects are usually present even within a freshly applied coating and can develop over time due to environmental degradation (water uptake, UV radiation, temperature, etc.) and service-related factors (mechanical loading, foreign object strikes, application error, etc.).
Electrolyte	Aqueous medium (usually with water as the solvent) which contains ionically charged aqueous species (such as Na ⁺ and Cl ⁻). An electrolyte is necessary for corrosion processes to provide ionic convection between anodes and cathodes by the transport of the charged ions in the aqueous phase. This is necessary to maintain electroneutrality. Electrolytes range in composition and concentration. In atmospheric exposure, thin film electrolyte layers of deliquesced salt films can be quite concentrated depending on the relative humidity.
Chemical inhibition	A corrosion protection mechanism by which electrolyte chemistry is altered to prevent or mitigate corrosion.
Metal-Rich Primer (MRP)	A component of an overall coating system which provides corrosion protection for substrates such as steel or aluminum via physical barrier properties, galvanic protection, and/or chemical inhibition. Metal-rich primers may be used in conjunction with surface pretreatments and topcoats.
Pigment	In the context of metal-rich primers, pigments are metal powders embedded in the resin to provide corrosion protection via cathodic protection, cathodic prevention, or chemical inhibition. The pigment volume concentration of a primer is a critical parameter by which metal-rich primers are designed.
Pigment Volume Concentration (PVC)	The volume fraction of the primer composed of metal pigments. Most primers have a critical PVC value at which coating effectiveness is optimized, which will depend on factors such as the type of resin, metal pigment, pigment geometry, and environment the primer will be exposed to.
Resin	The resin in a metal-rich primer is an organic or inorganic matrix which binds the metal pigments together.

with increasingly negative coupled potential, reduced coating resistivity, and increasing porosity (King and Scully, 2011). A high magnitude of galvanic protection via MRPs also requires high sacrificial particle connectivity within the MRP resin, as well as high ionic connectivity through resin wetting/porosity (King and Scully, 2011). For this reason, limiting ion ingress through use of topcoats, or limiting sacrificial particle connection with the substrate through use of pretreatments, may negatively affect the magnitude of galvanic performance achieved (King and Scully, 2011; Kannan et al., 2015). Corrosion product may also inversely affect galvanic performance through filling pore space or decoupling sacrificial particles, which is commonly observed to occur in ZnRPs (Abreu et al., 1996; Marchebois et al., 2002; Thomas et al., 2013). Thus, the resin porosity, resistivity, and sacrificial particle PVC must be balanced for galvanic protection performance which is long-lasting as well as high in magnitude.

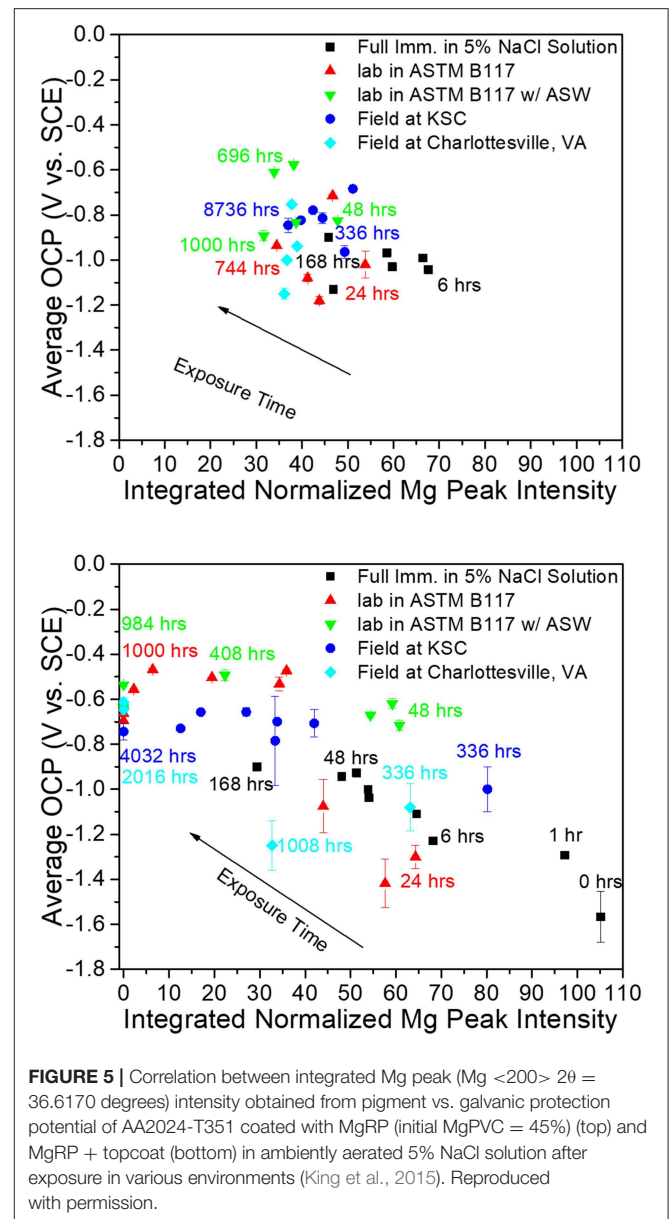
Comparison between ZnRPs has demonstrated that the use of high porosity resins such as ethyl silicate may achieve lower resin resistance than that seen in primers with similar Zn PVC but a less porous, more resistive organic resins (Feliu et al., 1993b; McMahon et al., 2019a). In MgRPs, increasing the resistivity through use of a topcoat or more resistive resin

has been demonstrated to reduce the self-corrosion rate of the sacrificial Mg, although the galvanic performance is suppressed also, meaning that a lower degree of galvanic control is achieved for a longer duration (Figure 5; King et al., 2014a). The effect of the resin for a similar Zn PVC may be balanced with the sacrificial particle size distribution, which influences the particle packing and overall connectivity (Vilche et al., 2002; Kalendová, 2003). The use of lamellar sacrificial particles has been demonstrated to achieve more effective packing and interconnectivity (Vilche et al., 2002; Kalendová, 2003), which directly affects overall primer conductivity (Wang, 2012). When utilizing spherical sacrificial particles, wider size distribution has a similar effect, which was demonstrated utilizing a combination of nanoscale-Zn and macroscale-Zn particles to increase interconnectivity and galvanic longevity on steel (Schaefer and Miszczyk, 2013). Of course, a combination of sacrificial particle types may also be utilized to fine-tune galvanic protection performance. Alloyed sacrificial particles such as Zn-Mg or Al-Zn have been evaluated to determine the exact compositions which achieve the optimal galvanic performance, with attention to the magnitude of galvanic couple potential achieved for the specific substrate as well as the subsequent corrosion product formation that occurs



to form a secondary barrier (Prosek et al., 2008; Plagemann et al., 2013; Wang et al., 2013; Salgueiro Azevedo et al., 2015; Stoullil et al., 2015). Additives have also been considered within the adhesive resin to increase conductivity, such as polyaniline emeraldine salt, silicone acrylate, and carbon nanotubes, among others (Armelin et al., 2010; Zhang et al., 2012; Cubides and Castaneda, 2016). Additionally, and important toward substrate protection, is the galvanic throwing power of the coating, whereby potential and current distributions are established by the galvanic coupling of a remote, exposed macro-defect to the MRP-coated substrate. In this way, the macro-defect is cathodically polarized by the coated substrate, achieving the desired potential control for protection of the susceptible substrate at the scribe for longer and longer scribe widths.

Metal-rich primers have also been considered for environmental fracture mitigation in the substrate material, which requires a high degree of galvanic protection to maintain effective coupled potentials at crack tips in the presence of tortuous crack paths with considerable IR drop. In short, environmental cracking has distinct critical thresholds (i.e., E_{crit} , T_{crit} , $[Cl^-]$) beyond which this phenomenon occurs, and these thresholds must be avoided. In the case of a primer, $E < E_{crit}$ is a criterion for protection. The ability of ZnRPs to maintain such potentials following aggressive simulated galvanic coupling in 0.6 M NaCl has been demonstrated to depend strongly on the aforementioned primer design characteristics such as sacrificial particle connectivity, porosity, resin resistivity, and more (McMahon et al., 2019a). The performance attribute that is most critical to the ability of an MRP to mitigate crack propagation via a galvanic mechanism besides the corrosion or galvanic couple potential is the pigment/primer polarizability, or the ability of the primer to maintain a cathodic electrode potential despite increasingly large exposed cathode areas (such as during crack growth) (McMahon et al., 2019a,c). This performance



attribute is complex, and depends on nearly the entirety of the previously discussed primer attributes and design characteristics: sacrificial particle type, loading, interconnectivity, and the resin (resistivity and porosity) (McMahon et al., 2019a). Optimally low polarizability is achieved through maximized anodic charge output in response to increasing cathodic surface area, with fast anodic response time maintained despite sacrificial particle oxidation and corrosion product formation. This level of performance may conceivably lead to a shorter MRP service life compared to those with higher impedance and lower anodic charge output. Thus, in environmental fracture scenarios, some of the desired MRP attributes for optimal mitigation performance may differ with respect to those desired for typical corrosion prevention situations.

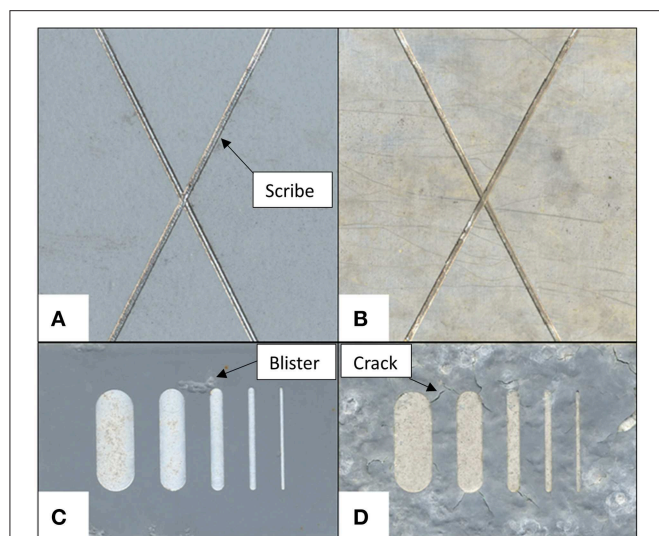


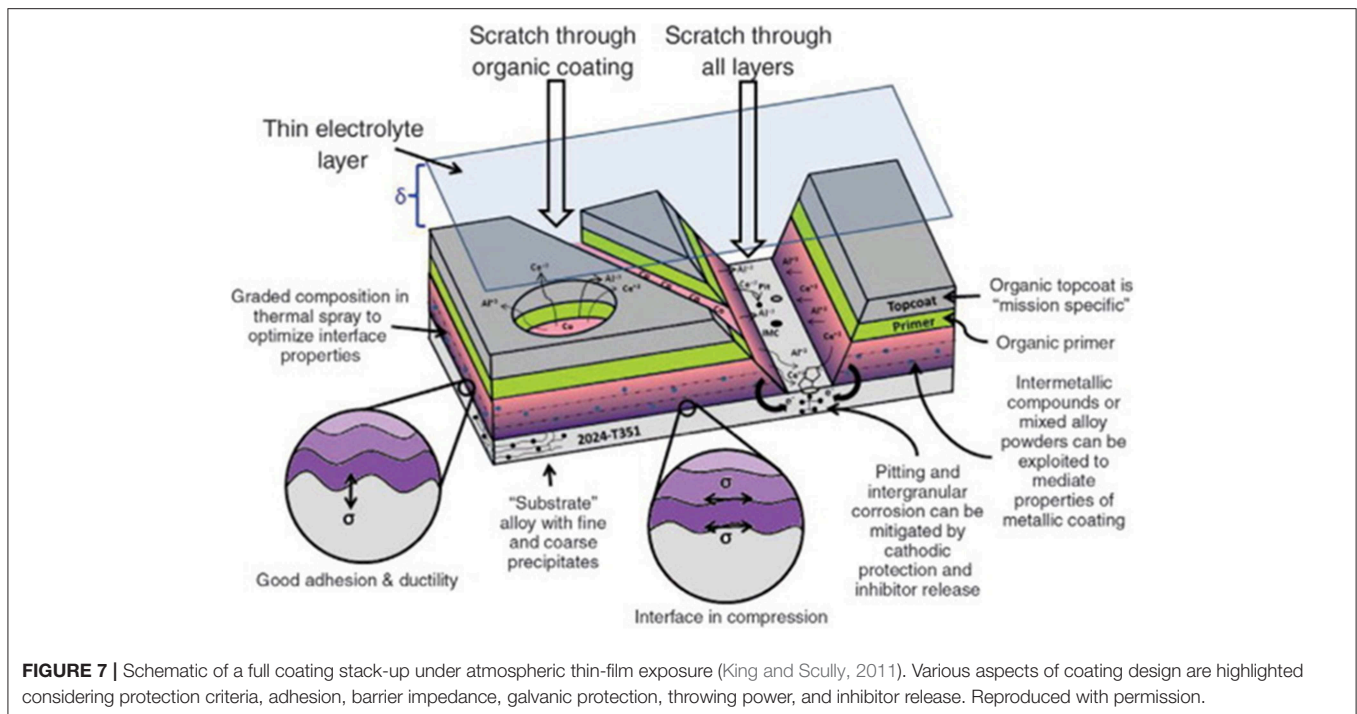
FIGURE 6 | Optical images exemplifying different types of coating defects, some of which are labeled. All coatings were deployed in field exposure testing with a machined scribe defect. In **(A)** a topcoated MgORP is shown after 2.5 years of exposure to Charlottesville, Va Birdwood golf course, and in **(B)** the same MgORP without a topcoat after being deployed in the same exposure conditions, resulting in the primer being completely degraded down to bare substrate. In **(C)**, one type of chromated primer is shown following exposure to Daytona, FL coastal marine environment for 3.2 years, exhibiting blistering in the coating, and in **(D)** a different chromate pigmented primer is shown following exposure to the same coastal environment, in which the coating exhibited severe cracking.

High Impedance Barrier

Coatings can function as a high impedance barrier to prevent high ionic conductivity enabled by electrolyte ingress to the substrate. Metal-rich primers maintaining high impedance act to impede the fast penetration of ions to drive corrosion reactions, and serve as a physical barrier (Leidheiser, 1982; Bellucci and Nicodemo, 1993). By preventing electrolyte contact with the substrate surface, the formation of a corrosion cell is prohibited and attack is circumvented. Barrier protection is promoted by good coating-substrate adhesion, resistive coating thickness, low defect density (as with pores), coating hydrophobicity, and slow coating degradation during exposure. A good barrier coating would allow no transport of species (ions, O₂, solvent, etc.) to or from the substrate surface. An imperfect coating can still mitigate corrosion damage by severely limiting the transport of current carrying species to and from the surface and between anodes and cathodes. The resin properties dictate such protection, specifically the crosslink density, since the restriction on chain mobility increases barrier properties (Leidheiser, 1982; Bierwagen, 1996; Sørensen et al., 2009). Recent works have also considered intrinsically conductive polymer-based coatings and their ability to maintain adequate barrier properties (Paliwoda-Porebska et al., 2005; Rohwerder et al., 2009, 2011). These findings have demonstrated that conductive polymer separation from the metal surface and macroscale percolation pathway formation must be avoided in order to mitigate a phenomenon

known as buried interface corrosion, wherein the metal-coating interface oxidizes as the coating promotes fast cation mobility to the metal surface (even in the absence of delamination) (Paliwoda-Porebska et al., 2005; Rohwerder et al., 2009, 2011). Over the course of an exposure, the barrier properties of both conductive and non-conductive coatings can degrade, most commonly by degradation of the polymer matrix (through dissolution into the electrolyte or UV radiation decomposition) or formation of transport pathways such as cracks, pores, etc. Field exposures tend to be very severe on organic coating matrices due to the effect of solar UV radiation on polymer decomposition, some examples of which are shown in **Figure 6**. This motivates the application of UV-resistant topcoats to be applied over the primer, which may reduce polymer degradation to extend the lifetime of the barrier properties. Even with a topcoat, however, electrolyte will inevitably penetrate the polymer network, which will reduce the primer impedance with time (Hack and Scully, 1991). For the purposes of reducing the ability of the ions to fully penetrate, the incorporation of inert inorganic or metallic particles may be beneficial when below the CPVC (Thomas, 1991; Koulombi et al., 1997). Above the CPVC, there is insufficient binder to fill the void between pigment particles, and/or there is a connected path along the particle interface and therefore the coating will be porous and have poor barrier properties (Thomas, 1991). Pigment or mineral filler particles such as titanium dioxide, micaceous iron oxide, glass flakes, lamellar aluminum, clay, silica etc. may be utilized to improve barrier properties of the coating. As far as the pigment shape is concerned, lamellar or flake particles are more effective compared to spherical pigments as they increase the tortuosity of the diffusion path prior to reaching the substrate when aligned perpendicular to the diffusion path (Moggridge et al., 2003; Yang et al., 2004). Stronger chemical bonding at the filler particle/resin interface also retards the electrolyte diffusion through the coating, which restrains electrochemical reactions on the underlying substrate. Furthermore, effective barrier coatings may also restrict the ingress of oxygen, which may slow cathodic reactions and thus the overall corrosion rate on the substrate (Walter, 1986; Sørensen et al., 2009; Glover et al., 2017). Restriction of the electrolyte and oxygen ingress may be achieved by a variety of primer formulations in various degrees, and will depend on the environmental exposure conditions (**Figure 5**; King et al., 2014a).

Without proper resin adhesion to the substrate, however, high impedance barrier properties are largely lost as the electrolyte can readily ingress. Proper substrate cleaning may promote proper primer adhesion (Marsh et al., 2001; Vakili et al., 2015). Commonly used pretreatment approaches include silanization, phosphating, application of conversion coatings, abrasive blasting, and anodization. The specific environment to which the primer will be exposed must also be considered. Temperature, pH, ultraviolet radiation, relative humidity, chloride content, as well as the presence of atmospheric pollutants such as nitrates and sulfates may all have deleterious effects on coating formulations, especially concerning the degradation of the barrier and adhesion properties (Mansfeld et al., 1982; Hack and Scully, 1991; Mansfeld and Tsai,

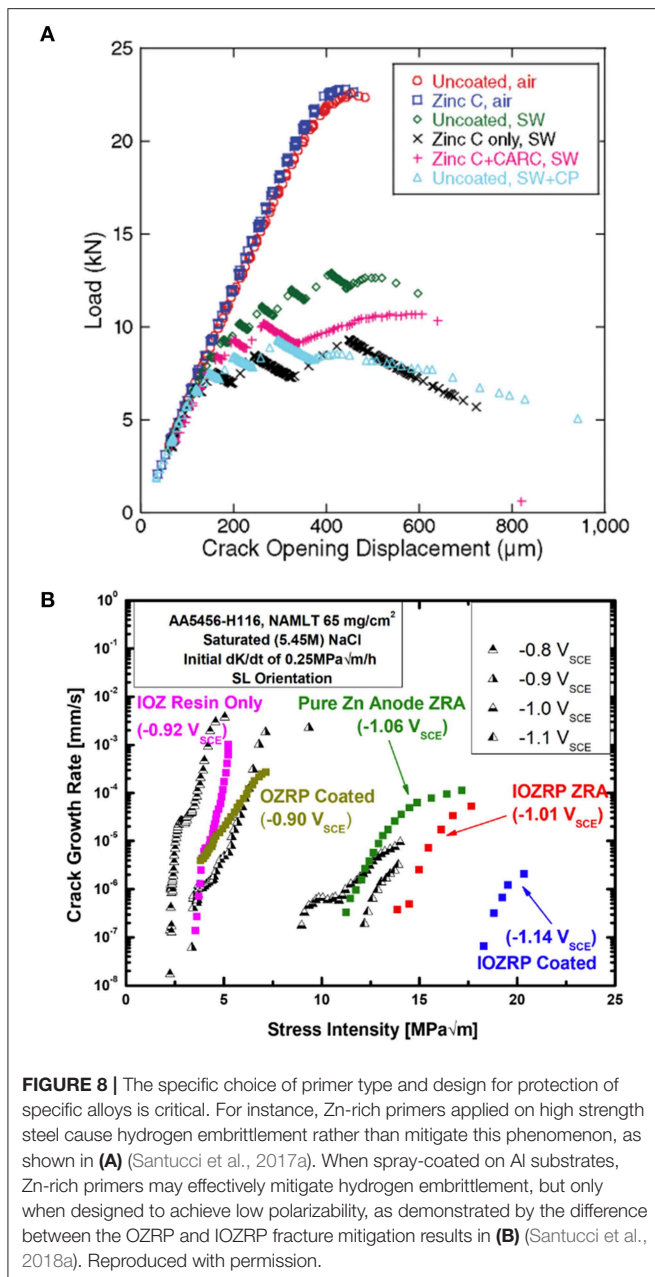


1991; Tayler et al., 2015a,b). The complex combinations of influences that these environmental factors may have on barrier performance are often understood for specific primer formulation types through use of laboratory-based accelerated life cycle testing (LALT) methods and field exposure, which will be discussed in an ensuing section.

Optimization and Effectiveness

Metal-rich primers typically operate through a combination of the previously discussed protection mechanisms. Optimization of MRP effectiveness is possible only through thoroughly understanding the environment to which the MRP will be subjected, the properties of the underlying substrate, resin properties, and the requirements for degradation mitigation. The array of these potential considerations on a substrate such as AA2024-T351 are demonstrated in **Figure 7** for a complex coating system (Presuel-Moreno et al., 2008). The resin properties such as ionic resistance and permeability to different detrimental species such as chloride, oxygen, water, anions, and cations will dictate the primer activation time as the sacrificial particles become increasingly connected with the external environment (Maier and Frankel, 2011). This was demonstrated by Maier et al. using an SKP to profile the interface between a bare substrate and an MRP (Maier and Frankel, 2011). Through a series of line scans across a thin aqueous electrolyte layer, it was shown that electrolyte must first penetrate the polymer network and the oxide layer on the embedded metal pigment before a galvanic couple was established and the metal pigment could function as a sacrificial anode. Once this galvanic couple was established, the magnitude of the established galvanic couple potential must be balanced so as not to be overly negative.

Inducing overly cathodic polarization may cause, rather than mitigate, hydrogen embrittlement phenomena in the substrate, as has been seen when utilizing ZnRPs on high strength steels (**Figure 8A**; Koul et al., 2014). When the potentials are in a passive polarization regime, the magnitude of coupled potential achieved on the substrate may drastically affect the rate of the prevailing degradation phenomena such as stress corrosion cracking, as has been demonstrated with ZnRPs on an Al-Mg alloy (**Figure 8B**; McMahon et al., 2019c). On amphoteric alloys such as Al, there is concern for the initiation of alkaline corrosion as well (Aballe et al., 2001; Tran et al., 2016). Alkaline corrosion phenomena may be especially severe when constituent particles intersect the alloy surface to act as fast cathodic reaction sites, which will form local alkaline regions that aggravate amphoteric substrate dissolution (Aballe et al., 2001, 2003; Huang and Frankel, 2007; Zhu et al., 2018; McMahon et al., in review). Thus, the barrier and galvanic properties of the MRP must be properly balanced to optimize performance for specific substrates, with particular attention to reducing the risk for exacerbation of degradation. As was discussed previously (and demonstrated in **Figure 4**), for a given resin resistivity, this may be achieved by tuning the PVC, or by adding a topcoat (which also provides UV weathering resistance) to increase overall resistivity (King and Scully, 2011; Kannan et al., 2015). The sacrificial particle composition may also be adjusted; for example, Plagemann et al. demonstrated on aluminum substrate that sacrificial particles composed of 74% Zn, 26% Mg achieved the optimal combination of galvanic coupling and self-corrosion rate (Plagemann et al., 2013). The variety of primer attributes which may affect overall performance through simple or complex relationships based on chemical inhibition, galvanic protection,



or high impedance creates a multitude of design avenues. For this purpose, mathematical models are in development to collectively assess the diversity of impartial metrics of MRP performance, which aim to inform effective MRP design (Ghafari et al., 2019). More traditionally, coatings are often vetted through exposure to LALT environments and protocols, or by field exposures. The LALT methods seek to duplicate the prevailing degradation mechanisms occurring in outdoor exposure, which requires a diversity of characterization techniques that must be collectively applied to assess performance. This is because degradation may be slighter in short term LALT even given acceleration, and this requires greater fidelity to assess. These points are discussed below.

METAL-RICH PRIMER ASSESSMENT METHODS

Outdoor Exposure/Accelerated Life Cycle Tests

Outdoor exposure and laboratory-based accelerated life cycle tests are some of the most direct testing methods available to predict MRP performance in service conditions. Examples of outdoor exposure methods include MRP panel exposure in coastal areas for years at a time, where the combination of UV degradation, salt spray deposits, and atmospheric pollution/precipitation may influence the overall performance. Geographically unique outdoor exposure locations will yield different levels of environmental severity and degradation in the substrate and the coating; thus, a combination of locations is often considered. In the laboratory, the methods described in ASTM B117 for accelerated salt fog testing, while quite imperfect at simulating outdoor environments, may be adjusted to best approximate service conditions through the maintained wetness of the chamber bottom, the duration of spray and drying cycles, as well as the acidification of the spraying solution (Parker et al., 2015; ASTM International, 2018). While salt fog testing can be indicative of the barrier performance of the coating under a thin film of electrolyte, it doesn't replicate the internal stresses, concentration and dilution of electrolytes developed in the coating during wet/dry cycles, or the higher temperature. So, performance of the coating in multiple accelerated testing approaches such as full immersion, continuous salt fog, cyclic corrosion testing, constant relative humidity exposure, a combination of UV and salt fog exposure, etc. are often necessary to mimic field performance (Tayler et al., 2015a,b). These various laboratory and outdoor exposures are often compared to assess the accuracy of a given laboratory-based method to realistic outdoor conditions, as well as to further understand the impact of environmental effects such as UV radiation and pollutants on coating degradation (Tayler et al., 2015a,b).

A suite of characterization methods must be employed to determine the correlation between accelerated exposure testing methods, such as LALT, and simulated corrosion testing on small-scale electrodes, such as direct current polarization, galvanic coupling, or electrochemical impedance spectroscopy (EIS). Tayler et al., for instance, utilized Raman spectroscopy, x-ray diffraction (XRD), 3-D optical microscopy, and more to demonstrate that UV exposure and wet/dry cycling are critical elements of LALT methods required to accurately correlate coating degradation to outdoor exposure (Tayler et al., 2015a). Polymer degradation is a primary concern following long-term MRP exposure, since UV-based photodegradation may compromise resin mechanical properties and adhesion to the substrate. Fourier transform infrared spectroscopy—attenuated total reflectance (FTIR-ATR) is a commonly utilized means to quantify the degree of degradation based on the reduction in reflectance observed when comparing spectra collected before and after coating exposure (Pathak et al., 2012; Tayler et al., 2015a; Petry and Hansen, 2016). Specifically,

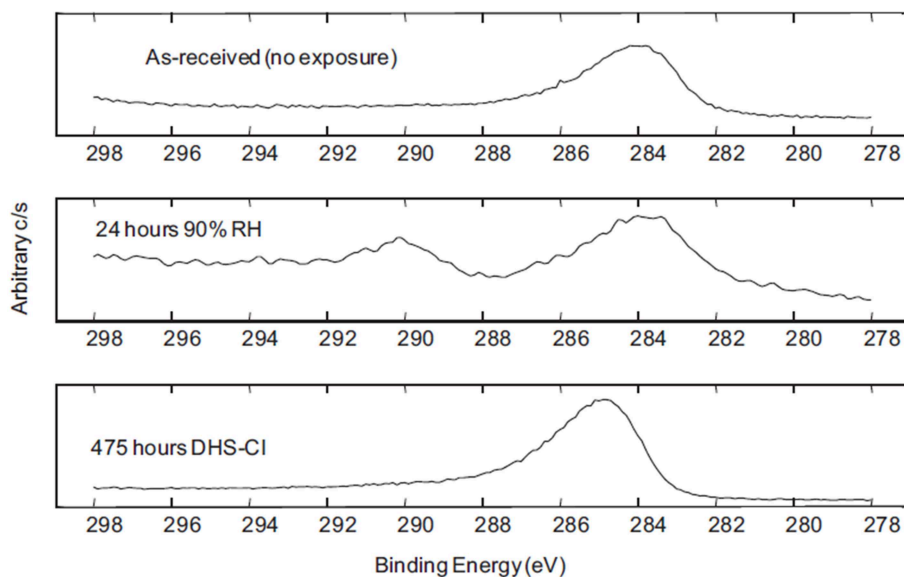


FIGURE 9 | X-Ray Spectroscopic analysis results demonstrating the development of C(1s) peaks over time of exposure in different simulated atmospheric conditions on the surface of a MgRP (Francis, 2013). Reproduced with permission.

this technique may indicate breakdown of primary and secondary amines resulting in degradation of polyurea and polyurethane functional groups. This technique allows for the direct comparison between outdoor exposures and LALT to determine if similar breakdown in primer resins or topcoats is achieved (Pathak et al., 2012; Petry and Hansen, 2016). X-ray diffraction provides evidence to understand the reduction in sacrificial anode (i.e., metal pigment) capacity (i.e., moles of metallic pigment remaining within the primer), which directly relates to subsequent galvanic performance often observed with time of outdoor or simulated outdoor exposure through comparison of sacrificial particle crystalline peak intensity (King and Scully, 2011; King et al., 2014a). Concerning MgRP systems having no topcoat or pretreatment, XRD has demonstrated that a complete loss of Mg content occurs following roughly 1,000 h exposure in ASTM B-117, and after roughly 24 weeks of exposure in marine/rural outdoor environments (King and Scully, 2011; King et al., 2014a). This disparity in achieved performance points out a current gap in the state-of-the-art, which is the lack of correlation between laboratory-based test methods and atmospheric exposure. Despite the complete loss of Mg peak intensity in XRD, studies have shown that MgRPs continue to protect an underlying Al substrate during outdoor exposure, which motivates more detailed assessment into corrosion product formation and alternative chemical protection effects (Santucci et al., 2017a).

Crystalline corrosion product may be effectively evaluated through a combination of bulk and surface-sensitive methods such as Raman spectroscopy, FTIR, XRD, and x-ray photoelectron spectroscopy (XPS), all of which provide either compositional or crystallographic details on the nature of

the precipitates (Pathak et al., 2010; Kannan and Scully, 2016; Santucci et al., 2017a). X-ray photoelectron spectroscopy and Raman spectroscopy are both especially useful for the sensitive detection of corrosion products and/or chemical modification on sacrificial pigment surfaces due to their penetration depth of as little as 5 nm, an example of which is shown in **Figure 9** for a MgRP surface (Park et al., 2012; Gergely et al., 2013; Jalili et al., 2015). The spatial resolution of XPS today, which can be on the order of 10 μm or less, may also aid the detection of corrosion product distribution into scribes and/or inhibitor coverages on remote alloy surfaces (Plagemann et al., 2013). Certain compounds may not have a Raman signature or may be difficult to detect, in which case the XPS precision and/or ability to deconvolute peaks is useful. Critical aspects of these techniques, as well as others essential to the characterization of coating performance, are provided in **Table 2**. Scanning electron microscopy (SEM) may also provide detail on the morphology and location of the precipitates, regardless of crystallinity, although chemical information by related methods such as energy dispersive spectroscopy (EDS) is spatially limited, and penetration depth is typically 1 μm or greater. For the MgRP system, this combination of methods demonstrated that Mg is converted into hydroxides during LALT, and becomes hydroxides as well as carbonates following outdoor exposure due to differences in the atmospheric conditions such as presence of more carbon dioxide (Pathak et al., 2010; Kannan and Scully, 2016; Santucci et al., 2017a). Due to the surface sensitivity of Raman and FTIR (Pathak et al., 2010, 2012; King et al., 2014a; Kannan et al., 2018a) and the identification of hydroxides via XRD (a method with considerably greater signal penetration depth) after long term field exposure (Santucci et al., 2018b), it can be concluded that Mg becomes converted

TABLE 2 | Table summarizing the various techniques discussed, as organized by principles of operation, detailing important characteristic of each.

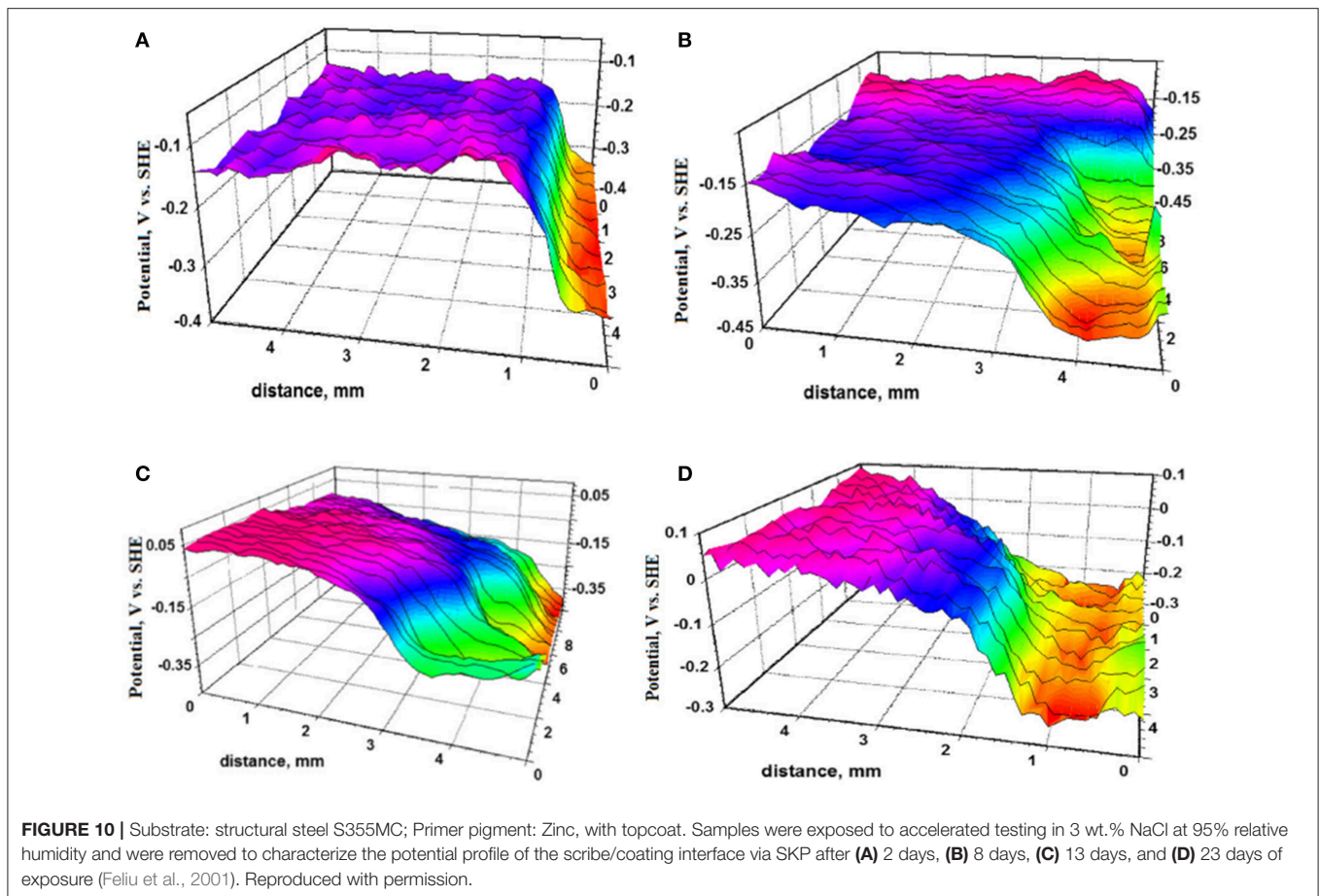
Principle of operation	Technique	Typical probe	Samples of interest	Interaction	Approximate energy difference	Typical signal	Diagnostic
Bohr Spectral Condition	FTIR	Infrared photon spectrum	Solid and aqueous	Vibrational and bending excitation	4–400 meV	Infrared photons	Molecular structure and bonding
	Raman	Single frequency visible and near-visible photons	Solid and aqueous	Inelastic Raman Scattering	1.5–3 eV	Frequency-shifted visible and near- visible photons	Molecular structure and bonding
	AES	Thermal Energy from Plasma or Arc	Aqueous	Electronic Excitation (Between Atomic Orbitals)	1–3 eV	Visible and near- visible photons	Inner shell atomic identification
	UV-Vis	Ultraviolet and Visible Photon Spectrum	Aqueous	Electronic Excitation (Between Molecular Orbitals)	1–100 eV	Ultraviolet and visible photons	Molecular structure and bonding
	EDS	Energized Electron Beam	Solid	Electronic Excitation (Between Atomic Orbitals)	0.1–100 keV	X-ray photons	Inner shell atomic identification
	XPS	Single Frequency X-ray photons	Solid	Electronic Excitation (Between Atomic Orbitals)	0.1–100 keV	X-ray photons	Inner and outer shell atomic identification
Bragg Diffraction Condition	XRD	Single frequency X-ray photons	Solid	Diffraction from Equivalent Lattice and X-ray Periodicity	NA	Single frequency X ray photons	Crystal structure and interplanar spacing
	P-EIS	Voltage perturbation spectrum	Electrochemical interface	Faradaic and Non-Faradaic Current Emission	$E = \frac{1}{2} CV^2$ where	Frequency-shifted current perturbation	Physical analogs to equivalent circuit elements (Corrosion Rate, Oxide Thickness, Coating Integrity, etc)
	G-EIS	Current perturbation spectrum			$C = I \div \frac{dV}{dt}$	Frequency-shifted voltage perturbation	

into magnesium hydroxide with a thermodynamically more stable magnesium carbonate surface layer (Santucci et al., 2018a). The combination of SEM and EDS has been utilized to evaluate pigment depletion and redeposition in coating scribes, which has been evidenced to increase with increasing exposure time during both LALT and outdoor exposure tests on MgRP/AA2024 (King et al., 2014a; Kannan and Scully, 2016; Santucci et al., 2017a). In acidified ASTM B-117 LALT, such Mg reposition and corrosion product formation in the scribe was limited compared to more neutral exposure conditions. The Mg corrosion products are simply more soluble in the acidified environment as indicated a variety of ways, notably chemical stability diagrams (Santucci et al., 2018a). In fact, chemical mapping of the redeposition zone by EDS¹ yields valuable insight into the throwing power and the extent of chemical protection achieved by MgRP as a function of environment (Kannan and Scully, 2016).

Once the scribe is cleaned of corrosion products and redeposited species, corrosion volume loss analysis in the scribe may further identify differences in primer performance as a function of environmental conditions. Classical techniques such as optical profilometry and confocal laser microscopy enable quantification of volume loss due to pitting in the scribe,

through which Kannan et al. demonstrated that the presence of the MgRP achieves corrosion protection on AA2024 more effectively in outdoor exposure than in neutral or acidified LALT (Kannan and Scully, 2016; Kannan et al., 2018b). More advanced evaluations in the laboratory may then further verify the differences in exposure conditions and MRP protection. For example, Nazarov et al. utilized scanning kelvin probe (SKP) on a scribed ZnRP to quantify location-specific potential changes that could be used for cross-evaluation with the corrosion volume loss results after as much as 23 days' immersion, which also directly demonstrated the suppression of pitting events and the MRP throwing power with time (Figure 10; Kannan et al., 2018b; Nazarov et al., 2018). Analyses utilizing SKP and complementary techniques such as EIS, scanning electrochemical microscopy (SECM), and more may also utilize SEM to visually confirm results, as has been demonstrated previously (Ogle et al., 2000; Volovitch et al., 2009, 2011; Marques and Simões, 2014). Electrochemical evaluation may offer further insight into the mechanisms driving long-term MRP performance. Embedded counter/reference electrodes may be placed between the primer and the topcoat, or between the primer and a pretreatment, to intermittently evaluate the state of the primer via EIS or measurement of the OCP during LALT, as long as these electrodes are resistant to chemical and environmental changes, do not alter the coating performance, and remain effective over extended periods of exposure (Prosek et al., 2008; King et al., 2014a; Merten et al., 2015). Embedded Ag/AgCl electrodes could be explored for this purpose (Rafla et al., 2018). Intermittent EIS has

¹It should be recognized that the EDS method is not surface sensitive and often has a depth of penetration of several micrometers, but the corrosion products deposited by homogeneous chemical precipitation are often several micrometers thick.



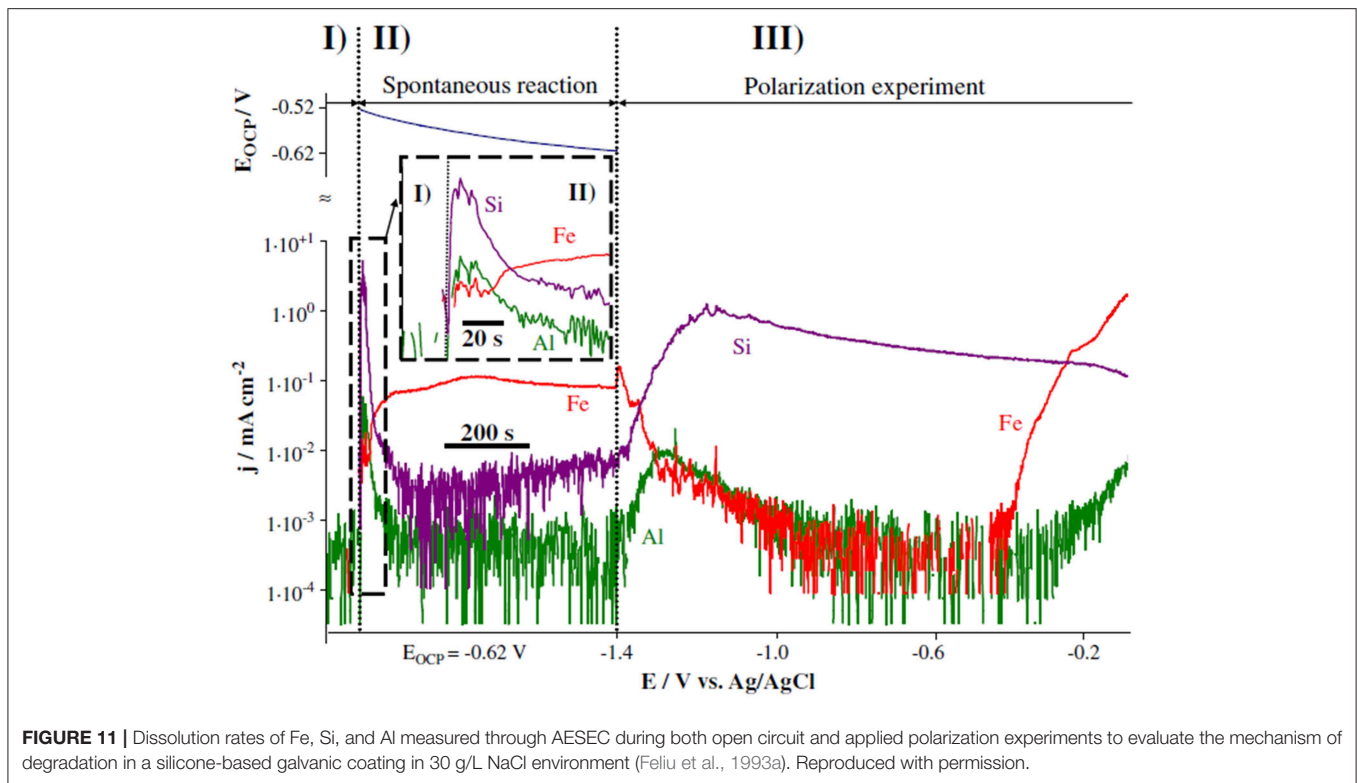
proven especially useful to understand changes in MRP porosity during long-term exposure when conducted at low frequency (0.01 Hz), and through evaluating the breakpoint frequency when conducted across a range of frequencies (Hack and Scully, 1991; Tsai and Mansfeld, 1993; King et al., 2014a).

Electrochemical Evaluation: Chemical Inhibition

Understanding chemical inhibition mechanisms often requires the quantification of the storage, dissolution, release, and transport of inhibitor species to a coating defect, such as a scribe. The delamination kinetics determined by the SKP technique via the measurement of changes in Volta potential difference underneath a scribed, coated sample provide an indirect indication of the effect of in-coating inhibitor species. The protection mechanism against underfilm cathodic delamination can be elucidated, such as: (1) chemical leaching from the coating; (2) the formation of permeation layers to block electron transfer to the cathodic site at the metal/coating interface; and (3) the formation of interfacial layers that increase the pathway for ionic mass-transport (Grundmeier et al., 2000). The SKP technique has been extensively utilized in the study of cation exchange within coatings, through which Williams et al. demonstrated that soluble chromate species are more effective when released from in-coating particulates such as SrCrO_4 because this enables

diffusion of CrO_4^{2-} directly into the under-film electrolyte layer (Williams et al., 2002, 2012). Scanning kelvin probe analysis has also demonstrated that cerium-based particles achieve more effective protection against delamination than simply adding Ce^{3+} to the bulk solution (Williams et al., 2002). To track the release of inhibitor species in solution, techniques such as ultraviolet-visible spectroscopy (UV-vis) may be utilized, which quantifies species concentrations and identifies species based on a characteristic absorption signature. The equilibrium fraction of soluble species will vary based on pH, as will the peak signal frequency and absorbance, as has been shown for Cr^{4+} (Xia et al., 2000). Moreover, identification of the isosbestic point, where absorbance is independent of pH, enables direct tracking of species concentration throughout exposure, which is a powerful capability. For cations that are not active in the UV-vis spectrum, active chelating agents may be added that selectively bind to certain cation types, even with sensitivity to the oxidation state (Shtoyko et al., 2007; Place, 2019). However, when adding chelators, the change of the resulting complex concentration as a function of cation concentration or pH must be understood.

Increasingly complex characterization methods are required to more fully understand the nature of chemical inhibitor-containing primer performance as a function of environment. Atomic emission spectroscopy (AES), which evaluates atomic concentration through exciting atoms contained within a



liquid medium and measuring the resulting photon emission during decay, has been adapted for this purpose (Hieftje, 2000). Inductively coupled plasma (ICP) atomic emission spectroelectrochemistry (ICP-AES) combines the atomic quantification of AES with the ability to control electrochemical conditions via potentiostatic or galvanostatic means, which has been utilized to understand conversion coating stability and substrate dissolution as a function of electrolyte composition (Ogle, 2004; Gharbi et al., 2016). An example of the results obtained on a silicone-based galvanic coating through ICP-AES analysis is shown in **Figure 11** (Ogle, 2004). This method may be coupled with SEM/EDS and Raman spectroscopy to characterize the deposition and/or precipitation of species of interest on the substrate surface, delivering a wholistic idea of the fate of chemical inhibitors from the initial dissolution within the primer. When small inhibitor concentrations are released from the primer, surface-enhanced Raman scattering (SERS) may also be utilized to identify precipitates if they exhibit a Raman signature (Zou et al., 1998; Oblonsky, 2006).

The release, transport, and redeposition of chemical inhibition species has been discussed thus far. The efficacy of these species toward reducing the corrosion rate of a given substrate must also be considered. One simple assessment commonly used is to monitor the mass loss of a known area of substrate exposed to an electrolyte with and without the inhibiting species. After exposure the substrate is subjected to a cleaning step in a process that is tailored to remove the corrosion product without further corroding the intact substrate (ASTM International, 1999). By correlating the mass loss of the substrate to corrosion damage,

a comparison can be made to determine if the inhibitor reduced the extent of damage, on the assumption that corrosion attack is uniform (i.e., not localized in morphology). This assessment is simple to conduct but cannot glean mechanistic understanding and cannot monitor the corrosion process during exposure. Potentiodynamic polarization testing is another well-utilized assessment. The measured current is related to the rate of oxidation and reduction according to Faraday's law and mixed potential theory. In the presence of an efficacious inhibitor, the measured currents should be lower than in the absence of the inhibitor. Alternating current assessments can be made with EIS as well. This measurement technique will be discussed in depth in the Theory and Modeling of Performance section of the review. For now, it is sufficient to note that the polarization resistance, which can be quantified via EIS, and which is related to the corrosion rate of the substrate by the Stern-Geary relationship, should increase in the presence of an effective inhibitor.

Galvanic Protection

The most basic means of directly measuring the magnitude of achieved galvanic protection is via the OCP² (Pereira et al., 1990; Feliu et al., 1993a, 2001; Danford et al., 1995; Hammouda et al., 2011; Santucci et al., 2017b; McMahon et al., 2019a). Feliu et al. have demonstrated, through intermittent OCP measurement, that ZnRPs can maintain galvanic protection on steels for 10

²Also referred to as the global galvanic couple potential to avoid confusion, the achievement of this value is rooted in mixed potential theory, which will be discussed in a section to follow pertaining to electrochemical modeling.

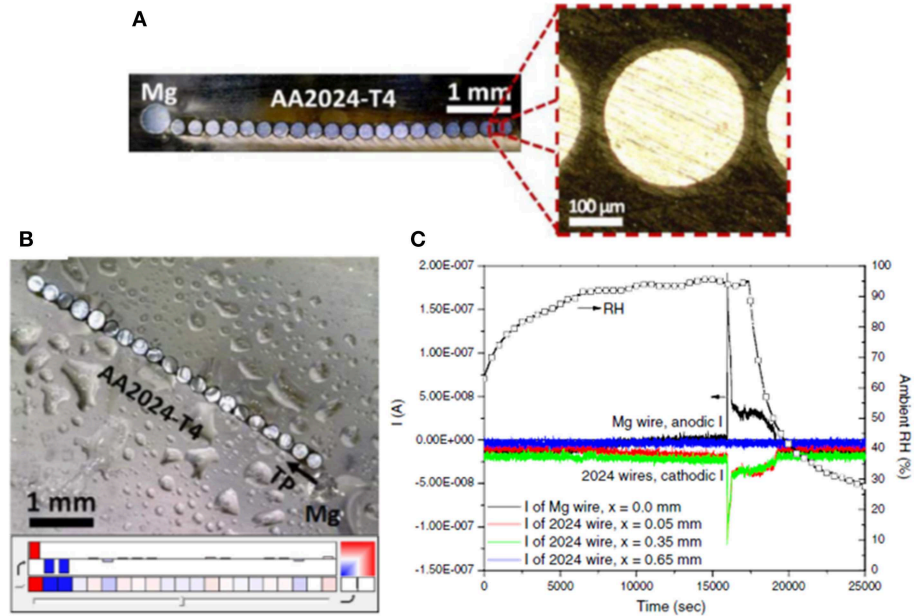


FIGURE 12 | (A) Optical images of a bare Mg/AA2024-T4 microelectrode array used to diagnostically assess the throwing power of Mg over a representative bare AA2024-T4 scratch in an RH controlled cabinet (Feliu et al., 1993b). The Mg electrode is 500 μm in diameter. The AA2024-T4 electrodes are 254 μm in diameter insulated by a 25 μm thick polyimide coating with a mean electrode spacing of 50 μm . The total width of all of the AA2024-T4 microelectrodes is approximately 5750 μm and the total area ratio of AA2024:Mg is 5:1. **(B)** optical image of the bare-Mg/bare AA2024-T4 microelectrode array with 1,000 $\mu\text{g}/\text{cm}^2$ NaCl deposited by salt spray and allowed to equilibrate at 94% RH for at least 3 h. In the color map dark red indicates an anodic current $\geq 1 \times 10^{-5}$ A/cm 2 and dark blue indicates a cathodic current of $\leq -1 \times 10^{-5}$ A/cm 2 . White color indicates a net current of zero. **(C)** Measured current and RH. Reproduced with permission.

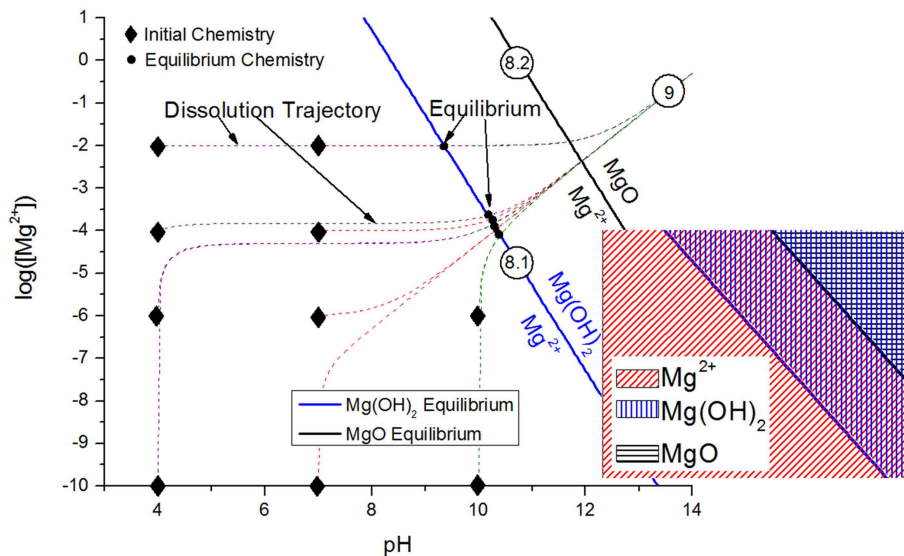


FIGURE 13 | Chemical stability diagrams detailing the ability of these thermodynamic derivations to predict corrosion product stability and conditions for formation in the Mg system (McMahon et al., 2019a). Reproduced with permission.

years in marine outdoor exposure, and the increase in the OCP past a critical threshold accurately predicts the onset of red rust due to known potential dependence (Feliu et al., 2001). When evaluating MRP-based galvanic protection for environmental

fracture mitigation, measurement of the galvanic couple potential on the exposed substrate surface with a nearby primer provides a rough estimate of the degree of protection achieved at a remote location such as the crack tip (McMahon et al., 2019c). In these

more aggressive scenarios, there may be a distance dependence to the galvanic couple potential, achieved due to the finite throwing power achievable via MRPs. Throwing power has been evaluated for several geometries and simulated conditions through use of multi-electrode arrays (MEAs) (King et al., 2015; Rafla and Scully, 2019). An example of an MEA consisting of pure Mg and AA2024-T351 electrodes (in this case, flush mounted wires were used to simulate a planar electrode) is shown in **Figure 12**, as well as an example dataset of currents achieved on various electrodes in salt spray (King et al., 2015). These custom setups enable the simulation of an exposed substrate area with embedded electrodes spaced throughout the exposed dimension, enabling localized current measurement to indicate where net anodic (if throwing power is ineffective at reaching such a distance) or net cathodic reactions are supported (when the throwing power is sufficient to distribute current to the electrode). The design of the electrode size and spacing is important where the dimension should enable potential and current field changes and/or consider anode-cathode microgalvanic couple sizes³.

These experimental evaluations are readily complemented by finite element analysis (FEA), which provides considerable insight on the effect of variables such as solution thickness and resin resistivity on the throwing power phenomenon (King et al., 2016). King et al. utilized FEA to demonstrate means through which MgRP throwing power may be improved on AA2024-T351 based on Mg polarization characteristics, solution thickness and resin resistance (King et al., 2016). The results of this analysis will be detailed further in an ensuing section. The scanning vibrating electrode technique (SVET) is another means of measuring throwing power. The use of SVET to make *in situ* localized corrosion current density distribution measurements in saline immersion was pioneered by H. Isaacs (Isaacs, 1988). The SVET enables the mapping of localized corrosion features occurring on metallic surfaces when fully immersed in aqueous media to discern physical size, shape, and spatial distribution. As such, quantitative anodic and cathodic current density data can be extracted via the numerical integration of SVET-derived current density (j_z) distributions and corrosion rates can be measured (Williams et al., 2010, 2013, 2014; Upadhyay and Battocchi, 2016; Fajardo et al., 2017). A wealth of literature exists documenting the use of SVET to monitor localized corrosion of bare metals and their alloys to elucidate fundamental corrosion mechanisms (Isaacs, 1988; Franklin et al., 1992; Williams et al., 2015). Furthermore, SVET is a very useful tool for the study of galvanic interactions between dissimilar metals (Deshpande, 2010; Yan et al., 2010; Coelho and Olivier, 2018; Glover et al., 2019) and, hence, for the evaluation of MRPs. An SVET study concerning the throwing power from a MgRP over an exposed AA2024 surface was able to locate the exact reach of sufficient galvanic coupling and the successful suppression of pitting (Kannan et al., 2018b). The SECM method has been similarly applied to study localized corrosion processes caused by galvanic coupling, where

galvanic protection may be assessed with high electrochemical sensitivity on the micrometer scale (Simoes et al., 2008; Izquierdo et al., 2013; Filotás et al., 2017; Xavier and Nishimura, 2017).

Primers having high sacrificial particle loading often have increased conductivity due to high particle interconnectivity, which may be measured through conductive atomic force microscopy (CAFM) (Bierwagen et al., 2007). This method differs from AFM by the application of a voltage from the tip to the sample surface, thus both a topographic map as well as a current map may be produced to identify (1) the distribution of conductivity at the surface (an indirect measure of metal particle proximity) as well as (2) the surface profile. This quantification method enables the researcher to determine the CPVC, the resin resistivity, and the sacrificial pigment connectivity without electrochemically testing the primer in an electrolyte (Bierwagen et al., 2007). Related to the conductivity is the MRP polarizability, which may be quantified through use of the newly developed galvanostatic pulse method (McMahon et al., 2019a). This technique consists of a cyclic repetition of applied anodic current having increasing magnitude, with intermediate OCP steps to assess the MRP's state of degradation/activation (McMahon et al., 2019a). Correlation of the polarizability of several ZnRPs based on a critical current threshold agreed with fracture mechanics-based assessment of these primers' performance in environmental fracture mitigation, showing promise as a fast screening method for the assessment of primers that must be capable of responding to sudden increases in bare substrate area which must be protected (McMahon et al., 2019a).

Theory and Modeling of Performance

Several modeling frameworks exist to predict and assess the performance of MRP systems. Typically, models are organized with respect to one of the three principal protection modes previously discussed: chemical inhibition, cathodic protection/prevention, or high impedance barrier protection. All three of these modes may be present in one coating system, though that is rare. Each modeling paradigm will be discussed by this scheme individually, and then synthesized into a discussion pertaining to all forms of protection.

Modeling of the storage, release, and accumulation of chemical inhibitors from coatings should be generally focused on the kinetics of inhibitor release, the transport, and the accumulation of the inhibitor species in some macro-defect in need of inhibition (such as a scribe or holiday). Inhibitor release kinetics are sensitive to the exposure environment, and proper model inputs need to capture this dependence. For chemical dissolution processes, the rate of dissolution is proportional to the degree of undersaturation of the species in solution with respect to the equilibrium conditions of compound stability (**Figure 2**). In this case, both the initial and final equilibrium inhibitor concentrations established by inhibitor dissolution are needed as model inputs, both to establish an upper bound on inhibitor delivery and also to inform chemical dissolution kinetics (Xia et al., 2000). For electrochemical dissolution processes, the kinetics are governed by electrode potential at the primer interface coping with any concentration gradients along with transport of cathodic species to be reduced on the electrode

³By definition the net array current will be zero at open circuit if all the anodes and cathodes reside on the same electrode. When anodic and cathodes are distributed and when there is a meso current and potential distribution the array provides useful information.

surface. The corrosion rate-determining techniques highlighted previously are useful here for determining electrochemical inhibitor release as a function of factors like pH and $[\text{Cl}^-]$ (Presuel-Moreno et al., 2006). The chemical release of Cr^{6+} from a chromate conversion coating (CCC) has been modeled utilizing a Langmuir adsorption-desorption mechanism (Xia et al., 2000; Akiyama et al., 2003). In this model, the CCC was simulated by a porous network consisting of solid chromate compound network and solution-penetrated pores. A Langmuir-type adsorption-desorption equilibrium was assumed between the solid network and the solution in the pore space to calculate a diffusion model for Cr^{6+} transport through the CCC into bulk solution (Akiyama et al., 2003). This assumed model adequately rationalizes experimental observations of Cr^{6+} release and final bulk Cr^{6+} concentration (Xia et al., 2000; Akiyama et al., 2003). Further considerations can be made to model the transport of inhibitor species from the coating to a defect like a scribe. In addition, achieving a critical inhibitor concentration for a large change in corrosion rate or to avoid a critical threshold potential are sometimes considered. Here the accumulation of the inhibitor such as over a scribe is tracked and a database is created on the change in “corrosion behavior” of the substrate alloy in response to the various inhibitor concentrations (Jakab et al., 2005; Presuel-Moreno et al., 2005a; Scully and Jakab, 2006). When the accumulated concentration over the scribe reaches or exceeds the critical level, the maximum level of protection is achieved.

The computational power of FEA has been utilized to model the long-range transport of Zn^{2+} and $\text{V}_{10}\text{O}_{28}^{6-}$ from an intact hydroxalcalite/vanadate coating to a scratch through the coating which exposes bare AA2024-T351 (Wang et al., 2004). Model inputs required experimentally determined, quantitative expressions of the anodic and cathodic kinetics of the AA2024-T351 substrate as a function of potential, and inhibitor concentration as well as the inhibitor release rate as a function of pH. Once developed, the model was able to assess the effect of scribe width, electrolyte film thickness, and pH on the concentration profile of the inhibitor species from the coating into a scribe over time (Wang et al., 2004). Furthermore, the same FEA modeling framework has been applied to protective metallic coatings which are designed to galvanically couple to the substrate both under the coating and within the scribe. The release of Ce^{3+} from an Al-Ce-Co metallic coating and the transport of Ce^{3+} from the coating into a scribe has also been modeled (Presuel-Moreno et al., 2006). In this case, an added migration term to Ce^{3+} transport due to the electric field was considered since the scribe can be negatively polarized by the intact coating. It was found that this migration term was significant enough to cause uphill transport of Ce^{3+} against the concentration gradient (Presuel-Moreno et al., 2006).

Galvanic coupling of the coated substrate to the uncoated substrate not only contributes to the migration of inhibitor species, but also acts to protect the exposed substrate by evoking electrode potential control. The motivation for employing cathodic protection having been discussed already, it is necessary to have computational tools with which to model the cathodic protection behavior of anodically-pigmented coatings. Finite

element techniques have been employed to spatially resolve the electrode potential and current distribution within a galvanically coupled scribe. The potential dictates the electrochemistry of the substrate, and also contributes to the transport of ions in solution, as previously discussed for the Al-Ce-Co coating system (Presuel-Moreno et al., 2006). The potential distribution has also been calculated for a scribed MgRP on AA2024-T351 to determine the galvanic throwing power of the coating, or the distance away from the intact coating over which significant potential control could be established in the exposed scribe (King et al., 2016). The effect of electrolyte composition, electrolyte layer thickness, polymer resistivity, and humidity cycling on the throwing power of MgRP was investigated. In general, it was found that throwing power was more extensive for more conductive electrolytes and polymer matrices and for a thicker or deeper electrolyte layer (King et al., 2016). Finite element model inputs relied heavily on experimental determination of the anodic and cathodic reaction rates (i.e., interface reaction rates) as a function of electrode potential, the thermodynamic dependency of the electrolyte layer concentration and physical thickness on the relative humidity and salt composition, as well as the geometry. A challenge with modeling primers is the resin resistance, which is an extremely important variable that must be contained in such models (even for a resin with the same resistivity at all positions) as a function of primer depth buried within the coating. In one approach, this was handled by assigning a depth beneath the primer surface to the pigment, and in other approaches there could be a distribution of depths.

A more generic framework than FEA exists in the mixed potential theory, which describes the galvanic coupling of two or more electrochemically distinct materials. The net anodic and cathodic current of each electrode is plotted as a function of electrode potential in proportion to the available area of each electrode (current is not area normalized). The contribution of current from each electrode is then summed to give the total net current of the system as a function of electrode potential (King and Scully, 2011; King et al., 2016). The electrode potential established on the surface depends on the anodic and cathodic kinetics of each electrode and also the resistance that exists between them. The resistance is proportional to the resistivity of the solution and the distance between the electrodes, giving rise to a geometric distribution of potential. The ohmic resistance which affects the electrode potential distribution is composed of the sum of all resistances between anodic pigments and the cathodic substrate (King and Scully, 2011). Resistance can arise from the solution, primer, topcoat, etc., with the high resistivity of the polymer coating matrix often contributing the most.

For a coating to function as a good barrier, it must prevent or limit either the ingress of the ionic species in the electrolyte to the coated substrate or the rate of anodic/cathodic reactions at the buried interface. Theoretically, a perfect coating would not accommodate any uptake of water or permeation of water to the substrate or transport of ionic species through the coating to and from the substrate. In reality, all coatings will instead suffer water permeation due to intrinsic coating defects (like pores) or developed defects (like cracks or scratches) (Leidheiser, 1982; Bellucci and Nicodemo, 1993). Current may

flow through the coating once it is sufficiently wetted with ionically conducting electrolyte. These coating defects provide low resistance pathways for current flow once saturated with electrolyte. In this way, the resistance of a coating is related to the tortuosity of the current path between anodes and cathodes, and it decreases with decreasing coating thickness as well as increases with wetting and defect development (Amand et al., 2013). Many techniques exist to assess the resistance (or barrier properties) of protective coatings in full immersion exposure. Electrochemical impedance spectroscopy is a commonly utilized technique, wherein an alternating current (AC) perturbation signal can be applied to a coated interface at a given current or potential amplitude centered at a given current or potential value, respectively (Orazem and Tribollet, 2017). When a potentiostatic EIS technique is deployed, for example, the resulting current response of the coated interface is measured. The AC response of the interface is dominated by the path of least resistance for current flow (or the path which gives rise to the lowest impedance response to the alternating potential). The electrochemical surface is composed of real physical elements which are either resistive, capacitive, or inductive in nature. Together, they give rise to an impedance response under AC conditions. The impedance response is a result of these circuit elements interacting together according to the laws which govern their individual behavior in response to alternating potential (or current) perturbations. Resistive elements which control current flow include solution resistance in the bulk electrolyte from the reference electrode to the coating, solution resistance within the pore space of the coating, and polarization resistance to electron transfer reactions at the electrochemical interface incorporating both the charge transfer and mass transport aspects (Mansfeld et al., 1982; Kendig and Scully, 1990; Mansfeld, 1990; Hack and Scully, 1991; Mansfeld and Tsai, 1991; Tsai and Mansfeld, 1993). Capacitive elements, which arise when charges are separated over a finite distance, affect impedance response as a function of perturbation frequency and include the Helmholtz double layer, coating capacitance, and oxide capacitance. Another example is the use of Warburg impedance elements to model real convective diffusional processes, which have a dual resistive and capacitive response to AC perturbations. A broadly applicable method such as EIS is not a universal means to understand all mechanisms of coating performance, and complementary combinations of techniques should always be considered; however, this method can be utilized in a variety of ways to gain valuable insight. It is worth noting that EIS is a global method biased by low parallel impedance and is not area specific (lacks spatial resolution). Overall, the impedance response of a coated system will depend upon the arrangement and magnitude of various resistors and capacitors, such that the electrochemical system can be modeled as an equivalent circuit (Orazem and Tribollet, 2017).

Equivalent circuit models are theoretical analogs to physical components of the electrochemical interface commonly constructed to simulate the impedance response measured by EIS. A least squares residual analysis is performed to vary the values of the various circuit elements to best fit the experimental data. Care must be taken to appropriately choose a representative equivalent circuit with physically significant parameters, some of

which are independently corroborated with to model a coated interface, as many different models could adequately fit the experimental data. For example, the impedance response of an oxide is more accurately comprised of the individual responses of many capacitors/resistors which sum to give the response of the actual oxide, giving rise to a capacitive dispersion. The oxide is not perfect and homogenous, but really inhomogeneous with respect to oxide thickness, oxide composition, oxide impurity concentration, oxide defect concentration, oxide crystallographic orientation, oxide grain boundaries, etc. In this case, it is too complicated to know or to model how all of these capacitances work together to give the impedance response of the cell. Instead, the sum behavior of the oxide capacitance is typically modeled as a constant phase element. Error analysis and independent verification is needed by complementary techniques to hone in on the values of the various elements (Orazem and Tribollet, 2008). Nested RC circuits utilizing two time constants have successfully been applied to impedance data of MgRP (King and Scully, 2011; King et al., 2014a,b; Kannan et al., 2015). Transmission line models have also successfully modeled MgRPs and ZnRPs (Allahar et al., 2008, 2010). In such cases, EIS can be effectively utilized to differentiate coating vs. buried interface corrosion, as a second time constant is developed upon environmental exposure which can be correlated to substrate corrosion. Equivalent circuit models are not only useful for theoretical fitting of EIS experimental data but also for theoretical fitting of potentiostatic pulse testing (PPT) data (Kang and Frankel, 2005). Since the transient current profile is a function of the time constants associated with the various capacitors in the system, equivalent circuit models can be constructed for PPT current transients to determine the value of various capacitive analogs (Kang and Frankel, 2005). This is of advantage over multi-frequency sweep sine EIS because instrumentation is often much more expensive than what would be required for PPT. However, the analytical power of EIS is much more robust than that of PPT, as EIS is able to probe the system over a very large range of frequencies to access more information about the coating system. Additionally, a scanning local electrochemical impedance spectroscopy (LEIS) apparatus has been used to measure all of the same key parameters as global EIS but on a spatially resolved scale with respect to coating defects like scribes and the progression of scribe creep as a function of exposure (Lillard et al., 1994; Jorcin et al., 2006). This is certainly an improvement over global EIS measurements.

Optimizing the protection performance of metal-based pigmented coatings is difficult due to the sometimes-conflicting characteristics which are desirable for good performance of each protection mechanism. Holistic frameworks have been developed to determine how to best maximize the corrosion protection of pigmented coatings. For example, barrier and inhibition protection must be carefully considered for coatings which contain metal-based inhibitor compounds. A framework has been considered to assess the selection of inhibitor pigments for corrosion protection (Sinko, 2001). For a given anion package, various metal cations can be selected to store the compound in the coating. While some beneficial corrosion inhibition effects have been observed for cations like Zn^{2+} (Krieg et al., 2012;

Liu et al., 2019), Mg^{2+} (Krieg et al., 2012; Liu et al., 2019), and Ce^{3+} (Kaesche, 1985; Jakab and Scully, 2005; Presuel-Moreno et al., 2005a, 2006; Ho et al., 2006; Scully and Jakab, 2006), the cation also influences the solubility of the compound and the subsequent pH of the solution due to hydrolysis (Sinko, 2001). While corrosion inhibition necessitates the release of the inhibiting ion, excessive solubility can be detrimental to coating barrier properties by excessive pore formation in volumes once occupied by pigments and also in blistering caused by the osmotic pressure differential (Sinko, 2001). This pressure differential may be established by electrolyte uptake into the coating, which is thermodynamically driven to dilute the high inhibitor concentration in the pore space (Sinko, 2001). In this way, an optimal pigment solubility (and usually solution pH) is required where inhibition is achieved (inhibitor concentration exceeds the critical concentration for inhibition) but osmotic blistering avoided (inhibitor concentration does not exceed the threshold for onset blistering). The solubility of metal-based compounds as a function of pH, constituent concentration, and chloride concentration is easily represented by the chemical stability diagram (Santucci et al., 2018a; McMahon et al., 2019b). Establishment of these diagrams allows for easy comparison of the equilibrium conditions for the formation and dissolution of compounds. Included in this framework, are calculation for determining how the solution chemistry (in terms of pH and metal ion concentration) progresses from some initial condition to some final, equilibrium condition (Santucci et al., 2018a; McMahon et al., 2019b). Analysis with chemical stability diagrams has proven useful for interpreting the behavior of Mg and Zn-based coating systems (Santucci et al., 2018a; McMahon et al., 2019b). An example of a chemical stability diagram for the Mg system is given in **Figure 13**.

As another example, barrier properties and cathodic protection must be carefully balanced to achieve optimal protection. The barrier protection of a coating is most effective when the coating contains a small fraction of defects which allow for electrolyte uptake in the coating and wetting of the substrate. However, this increases the resistance of the coatings, and in turn, the resistance between the anodic pigments and the cathodic substrate. As barrier properties increase, the efficacy of cathodic protection is mitigated. This has been observed for MgRPs which contain resistive topcoats and pretreatments (King et al., 2014a,b; Kannan et al., 2015; Kannan and Scully, 2016; Santucci et al., 2017a,b) and ZnRP containing various organic and inorganic polymer matrices (Knudsen et al., 2001, 2005; McMahon et al., 2019a). In this way, a balance must be struck between barrier performance and cathodic protection. Due to the difficulty in designing fully optimized coating systems, final formulations are often determined by Edisonian-type trial and error performance analysis in various field or laboratory-accelerated exposures. Even then, it becomes difficult to determine the best formulation for a given application due to the varied nature of service condition exposures and also the different lifetimes at which each type of corrosion protection dominates. For this reason, it is useful to employ mathematical ranking methods and decision-making theories to impartially determine the best formulation for a given application (Athanasopoulos et al., 2009; Ghafari et al.,

2019). When desirable attributes of a corrosion resistant coating are known (as delineated above), and experimental results of exposure analysis collected, they can be used as model inputs with which to rank the various formulations against each other. Numerical ranking methods have been applied to a composite zirconia coating on AA7057 to impartially determine what inhibitor package (null, Ce, or BTA) best protects the AA7057 substrate (Ghafari et al., 2019) according to the corrosion rate, corrosion potential, and impedance response, for example.

SUMMARY AND FUTURE PROSPECTS

Metal-rich primers operate through multiple modes of protection, many times in combination to protect the substrate, which has proven challenging to collectively characterize and thoroughly understand to guide further innovation. It is clear that multi-probe spatially resolved methods must be combined to obtain chemical, materials, electrochemical and physical characteristics. Further complexity lies in the timing, as the activation of sacrificial particles may be delayed by design or accidentally depending on the coating's purpose. In the case of pretreatments, the resistive layer might degrade enabling better contact between the primer particles and the substrate. One dominant mode of protection may transition into another as well, such as when galvanic protection ceases due to corrosion product filling of pore spaces, which then promotes better primer barrier properties. However, pigment passivation could be detrimental, thus these mechanisms often have to be balanced for optimal performance. Coating designers should think in terms of the coating attributes desired and then collectively design for them, rather than selecting coating stack ups piecemeal according to surface preparation, pretreatment, primer and topcoat. As MRPs progress in performance and complexity, a thorough understanding of characterization methods ranging across numerous length scales will be increasingly necessary. It is important to note that contemporary coating analysis such as by EIS in isolation is inadequate to assess all aspects of primer performance. For the purposes of this review, many of the previously discussed techniques are summarized in **Table 2** to assist the reader in understanding the role of each method. Unique combinations of experimental methods and characterization techniques must be increasingly utilized together or concurrently to further reveal the mechanisms enabling MRP performance (King et al., 2014a; Santucci et al., 2017a,b). The large datasets created through such work will then be well-suited for computer-aided performance ranking and coating selection models.

The global high performance anti-corrosion coating market, which was valued at US\$11.95 billion in 2014, is anticipated to grow 4.8% per year to reach US\$18.22 billion by 2023 (CNBC, 2016). Research on and development of new-age coatings will increasingly solidify the important position that these systems hold in combatting the significant loss of infrastructure due to corrosion while further reducing their environmental impact. As emission regulations tighten and industrial leaders continually strive to conform while continuing to improve

corrosion protection, modern coatings may be amongst the first products which incorporate new polymer resin formulations, alloys, and additives to meet increasingly stringent performance demands. Trial- and-error type studies and lessons-learned-approaches require too much time to enable rapid insertion of new technologies. The need for new coating solutions, such as will often be driven by changing environmental regulations, new substrates, and harsher environments, requires high fidelity methods in tandem, interactive analysis, and rapid feedback combined with accelerated testing. The issue of accelerated testing accuracy will remain of great importance, innovation will continue to push the envelope of modern understanding on the mechanisms of anti-corrosion coating performance, and increasingly diverse characterization techniques will be required to push further advancement. In addition, it is clear that artificial intelligence will be required such as neural network methods in order to establish relationships between many variables, test metrics, and long-term coating performance.

AUTHOR CONTRIBUTIONS

All authors contributed to the literature review and the structuring of the manuscript. JS oversaw and edited

the development and production of the manuscript. BK and ZW conducted the literature review of accelerated and outdoor exposure test methods. CG conducted the literature review of a variety of modern characterization methods such as scanning kelvin probe for the study of chemical inhibition and cathodic protection. RS conducted the literature review on chemical inhibition and modeling methods, and composed the section on modeling of coatings as well as portions of the manuscript detailing electrochemical impedance spectroscopy. MM conducted the literature review on galvanic protection and drafted the manuscript.

ACKNOWLEDGMENTS

The authors would like to thank the Office of Naval Research (Airan Perez, Award #N000-14-15-1-2491), the Office of the Undersecretary of Defense Corrosion University Pilot Program (Daniel Dunmire, Awards #FA7000-18-2-0006 and #FA7000-14-2-0010), the National Science Foundation under NSF DMR #1309999, and the Army Research Office under agreement #W911NF-14-2-0005 for the financial support enabling this work.

REFERENCES

- Aballe, A., Bethencourt, M., Botana, F. J., Cano, M. J., and Marcos, M. (2001). Localized alkaline corrosion of alloy AA5083 in neutral 3.5% NaCl solution. *Corros. Sci.* 43, 1657–1674. doi: 10.1016/S0010-938X(00)00166-9
- Aballe, A., Bethencourt, M., Botana, F. J., Cano, M. J., and Marcos, M. (2003). Influence of the cathodic intermetallics distribution on the reproducibility of the electrochemical measurements on AA5083 alloy in NaCl solutions. *Corros. Sci.* 45, 161–180. doi: 10.1016/S0010-938X(02)00067-7
- Abreu, C. M., Izquierdo, M., Keddad, M., N6voa, X. R., and Takenouti, H. (1996). Electrochemical behaviour of zinc-rich epoxy paints in 3% NaCl solution. *Electrochim. Acta* 41, 2405–2415. doi: 10.1016/0013-4686(96)00021-7
- Akiyama, E., Markworth, A. J., Mccoy, J. K., Frankel, G. S., Xia, L., and McCreery, R. L. (2003). Storage and release of soluble hexavalent chromium from chromate conversion coatings on Al Alloys: kinetics of release. *J. Electrochem. Soc.* 150, B83–B91. doi: 10.1149/1.1537755
- Aldykewicz, A. J., Isaacs, H. S., and Davenport, A. J. (1995). The Investigation of cerium as a cathodic inhibitor for aluminum-copper alloys. *J. Electrochem. Soc.* 142, 3342–3350. doi: 10.1149/1.2049985
- Allahar, K. N., Battocchi, D., Bierwagen, G. P., and Tallman, D. E. (2010). Transmission line modeling of EIS data for a Mg-Rich Primer on AA 2024-T3. *J. Electrochem. Soc.* 157:C95. doi: 10.1149/1.3274206
- Allahar, K. N., Hinderliter, B. R., Tallman, D. E., and Bierwagen, G. P. (2008). Water transport in multilayer organic coatings. *J. Electrochem. Soc.* 155:F201. doi: 10.1149/1.2946429
- Amand, S., Musiani, M., Orazem, M. E., P6b6re, N., Tribollet, B., and Vivier, V. (2013). Constant-phase-element behavior caused by inhomogeneous water uptake in anti-corrosion coatings. *Electrochim. Acta* 87, 693–700. doi: 10.1016/j.electacta.2012.09.061
- Armelin, E., Marti, M., Liesa, F., Iribarren, J. I., and Aleman, C. (2010). Partial replacement of metallic zinc dust in heavy duty protective coatings by conductive polymer. *Prog. Org. Coatings*. 69, 26–30. doi: 10.1016/j.porgcoat.2010.04.023
- ASTM International (1999). *G1-03(2017)e1 Standard Practice for Preparing, Cleaning, and Evaluating Corrosion Test Specimens*. West Conshohoken, PA: ASTM International. doi: 10.1520/G0001-03R17E01
- ASTM International (2018). *B117-18: Standard Practice for Operating Salt Spray (Fog) Apparatus*. West Conshohocken, PA: ASTM International. doi: 10.1520/B0117-18
- Athanasopoulos, G., Riba, C. R., and Athanasopoulou, C. (2009). A decision support system for coating selection based on fuzzy logic and multi-criteria decision making. *Expert Syst. Appl.* 36, 10848–10853. doi: 10.1016/j.eswa.2009.01.016
- Barker, R., Burkle, D., Charpentier, T., Thompson, H., and Neville, A. (2018). A review of iron carbonate (FeCO₃) formation in the oil and gas industry. *Corros. Sci.* 142, 312–341. doi: 10.1016/j.corsci.2018.07.021
- Bastos, A. C., Quevedo, M. C., and Ferreira, M. G. S. (2016). Investigating the separation of anodic and cathodic defects in organic coatings applied on metal substrates. An experimental contribution. *Prog. Org. Coatings* 96, 26–31. doi: 10.1016/j.porgcoat.2015.12.016
- Bellucci, F., and Nicodemo, L. (1993). Water transport in organic coatings. *Corrosion* 49, 235–247. doi: 10.5006/1.3316044
- Bierwagen, G., Allahar, K., Hinderliter, B., and Jung, H. (2007). “Zn-Rich coatings revisited,” in *Tri-Service Corros Conference* (Denver, CO).
- Bierwagen, G. P. (1996). Reflections on corrosion control by organic coatings. *Prog. Org. Coatings*. 28, 43–48. doi: 10.1016/0300-9440(95)00588-9
- CNBC (2016). *High Performance Anti-corrosion Coatings Market to reach US\$18.22 bn by 2023; Product Segment, End-User and Global Regional Analysis by Transparency Market Research*. Available online at: <https://www.cnbcm.com/2016/04/11/globe-newswire-high-performance-anti-corrosion-coatings-market-to-reach-us1822-bn-by-2023-product-segment-end-user-global-regional.html>
- Coelho, L. B., and Olivier, M. (2018). The inhibition efficiency of different species on AA2024/graphite galvanic coupling models depicted by SVET. *Corros. Sci.* 136, 292–303. doi: 10.1016/j.corsci.2018.03.015
- Cubides, Y., and Castaneda, H. (2016). Corrosion protection mechanisms of carbon nanotube and zinc-rich epoxy primers on carbon steel in simulated concrete pore solutions in the presence of chloride ions. *Corros. Sci.* 109, 145–161. doi: 10.1016/j.corsci.2016.03.023
- Danford, M. D., Walsh, D. W., and Mendrek, M. J. (1995). *The Corrosion Protection of 2219-T87 Aluminum by Organic and Inorganic Zinc-Rich Primers*. Huntsville, AL: NASA Report.

- Deshpande, K. B. (2010). Validated numerical modelling of galvanic corrosion for couples : magnesium alloy (AE44)– mild steel and AE44 – aluminium alloy (AA6063) in brine solution. *Corros. Sci.* 52, 3514–3522. doi: 10.1016/j.corsci.2010.06.031
- Fajardo, S., Glover, C. F., Williams, G., and Frankel, G. S. (2017). The evolution of anodic hydrogen on high purity magnesium in acidic buffer solution. *Corrosion* 73, 482–493. doi: 10.5006/1.3290386
- Feliu, J. S., Morcillo, M., and Feliu, S. (2001). Deterioration of cathodic protection action of zinc-rich paint coatings in atmospheric exposure. *Corrosion* 57, 591–597. doi: 10.5006/1.3290386
- Feliu, S. J., Barajas, R., Bastidas, J. M., Morcillo, M., and Feliu, S. (1993b). Study of protection mechanisms of zinc-rich paints by electrochemical impedance spectroscopy, electrochem. *Impedance Anal. Ans Interpret.* 1188, 438–449. doi: 10.1520/STP18084S
- Feliu, S. J., Morcillo, M., Bastidas, J. M., and Feliu, S. (1993a). Evolution of the protective mechanisms of zinc-rich paints during atmosphere exposure. *J. Coatings Technol.* 65, 43–48.
- Filotás, D., Izquierdo, J., Kiss, A., Nagy, L., Nagy, G., and Souto, R. M. (2017). Improved potentiometric SECM imaging of galvanic corrosion reactions. *Corros. Sci.* 129, 136–145. doi: 10.1016/j.corsci.2017.10.006
- Francis, R. A. (2013). “Inorganic zinc silicate coatings - the early days part II: the morgan whyalla pipeline,” in *Inorg. Zinc Coatings Hist. Chem. Prop. Appl. Altern., 2nd edition*, ed R. A. Francis (Victoria: The Australasian Corrosion Association Incorporated), 18–23.
- Frankel, G. S., and McCreery, R. L. (2001). Inhibition of al alloy corrosion by chromates. *Interface-Electrochemical Soc.* 10, 34–39.
- Frankel, G. S., Vienna, J. D., Lian, J., Scully, J. R., Gin, S., V., et al. (2018). A comparative review of the aqueous corrosion of glasses. Crystalline ceramics, and metals. *Npj Mater. Degrad.* 15, 1–17. doi: 10.1038/s41529-018-0037-2
- Franklin, M. J., White, D. C., and Isaacs, H. S. (1992). A study of carbon steel corrosion inhibition by phosphate ions and by an organic buffer using a scanning vibrating electrode. *Corros. Sci.* 33, 251–260. doi: 10.1016/0010-938X(92)90149-W
- Gergely, A., Bertóti, I., Török, T., Pfeifer, É., and Kálmán, E. (2013). Corrosion protection with zinc-rich epoxy paint coatings embedded with various amounts of highly dispersed polypyrrole-deposited alumina monohydrate particles. *Prog. Org. Coatings.* 76, 17–32. doi: 10.1016/j.porgcoat.2012.08.005
- Ghafari, A., Yousefpour, M., and Shanaghi, A. (2019). Corrosion protection determine of ZrO₂ / AA7057 nanocomposite coating with inhibitor using a mathematical ranking methods. *Appl. Surf. Sci.* 465, 427–439. doi: 10.1016/j.apsusc.2018.09.110
- Gharbi, O., Birbilis, N., and Ogle, K. (2016). In-Situ Monitoring of alloy dissolution and residual film formation during the pretreatment of Al-Alloy AA2024-T3. *J. Electrochem. Soc.* 163, C240–C251. doi: 10.1149/2.1121605jes
- Gharbi, O., Thomas, S., Smith, C., and Birbilis, N. (2018). Chromate replacement: what does the future hold? *Npj Mater. Degrad.* 12, 23–25. doi: 10.1038/s41529-018-0034-5
- Glover, C. F., Cain, T. W., and Scully, J. R. (2019). Performance of Mg-Sn surface alloys for the sacrificial cathodic protection of Mg alloy AZ31B-H24. *Corros. Sci.* 149, 195–206. doi: 10.1016/j.corsci.2019.01.015
- Glover, C. F., Richards, C., Baker, J., Williams, G., and McMurray, H. N. (2017). In-coating graphene nano-platelets for environmentally-friendly corrosion protection of iron. *Corros. Sci.* 114, 169–172. doi: 10.1016/j.corsci.2016.11.009
- Grundmeier, G., Schmidt, W., and Stratmann, M. (2000). Corrosion protection by organic coatings : electrochemical mechanism and novel methods of investigation. *Electrochim. Acta.* 45, 2515–2533. doi: 10.1016/S0013-4686(00)00348-0
- Hack, H. P., and Scully, J. R. (1991). Defect area determination of organic coated steels in seawater using the breakpoint frequency method. *J. Electrochem. Soc.* 138, 33–40. doi: 10.1149/1.2085574
- Hammouda, N., Chadli, H., Guillemot, G., and Belmokre, K. (2011). The corrosion protection behaviour of zinc rich epoxy paint in 3% NaCl solution. *Adv. Chem. Eng. Sci.* 01, 51–60. doi: 10.4236/aces.2011.12009
- Hellmann, R., and Tisserand, D. (2006). Dissolution kinetics as a function of the Gibbs free energy of reaction: An experimental study based on albite feldspar. *Geochimica* 70, 364–383. doi: 10.1016/j.gca.2005.10.007
- Hieftje, G. M. (2000). Atomic emission spectroscopy — it lasts and lasts and lasts. *J. Chem. Educ.* 77, 577–583. doi: 10.1021/ed077p577
- Ho, D., Brack, N., Scully, J., Markley, T., Forsyth, M., and Hinton, B. (2006). Cerium dibutylphosphate as a corrosion inhibitor for AA2024-T3 aluminum alloys. *J. Electrochem. Soc.* 153, B392–B401. doi: 10.1149/1.2217260
- Huang, T.-S., and Frankel, G. S. (2007). Effects of temper and potential on localized corrosion kinetics of aluminum alloy 7075. *Corrosion* 63, 731–743. doi: 10.5006/1.3278422
- Ilevbare, G. O., and Scully, J. R. (2001). Mass-transport-limited oxygen reduction reaction on AA2024-T3 and selected intermetallic compounds in chromate-containing solutions. *Corrosion* 57, 134–152. doi: 10.5006/1.3290339
- Isaacs, H. S. (1988). The measurement of the galvanic corrosion of soldered copper using the scanning vibrating electrode technique. *Corros. Sci.* 28, 547–558. doi: 10.1016/0010-938X(88)90023-6
- Izquierdo, J., Nagy, L., González, S., Santana, J. J., Nagy, G., and Souto, R. M. (2013). Resolution of the apparent experimental discrepancies observed between SVET and SECM for the characterization of galvanic corrosion reactions. *Electrochem. Commun.* 27, 50–53. doi: 10.1016/j.elecom.2012.11.002
- Jakab, M. A., Little, D. A., and Scully, J. R. (2005). Experimental and modeling studies of the oxygen reduction reaction on AA2024-T3. *J. Electrochem. Soc.* 152, B311–B320. doi: 10.1149/1.1949047
- Jakab, M. A., and Scully, J. R. (2005). On-demand release of corrosion-inhibiting ions from amorphous Al-Co-Ce alloys. *Nat. Mater.* 4, 667–670. doi: 10.1038/nmat1451
- Jakab, M. A., and Scully, J. R. (2008). Effect of pH and chloride ion concentration on inhibitor storage in amorphous Al-Co-Ce Alloys. *Corrosion* 64, 198–209. doi: 10.5006/1.3278466
- Jalili, M., Rostami, M., and Ramezanzadeh, B. (2015). An investigation of the electrochemical action of the epoxy zinc-rich coatings containing surface modified aluminum nanoparticle. *Appl. Surf. Sci.* 328, 95–108. doi: 10.1016/j.apsusc.2014.12.034
- Jorcin, J. B., Aragon, E., Merlatti, C., and Pèbère, N. (2006). Delaminated areas beneath organic coating: a local electrochemical impedance approach. *Corros. Sci.* 48, 1779–1790. doi: 10.1016/j.corsci.2005.05.031
- Kaesche, H. (1985). *Metallic Corrosion: Principles of Physical Chemistry and Current Problems, 2nd edition*. Houston, TX: NACE International.
- Kalendová, A. (2003). Effects of particle sizes and shapes of zinc metal on the properties of anticorrosive coatings. *Prog. Org. Coatings.* 46, 324–332. doi: 10.1016/S0300-9440(03)00022-5
- Kang, J., and Frankel, G. S. (2005). Potentiostatic pulse testing for assessment of early coating failure. *Z. Phys. Chem.* 219, 1519–1537. doi: 10.1524/zpch.2005.219.11.1519
- Kannan, B., Glover, C. F., McMurray, H. N., Williams, G., and Scully, J. R. (2018b). Performance of a magnesium-rich primer on pretreated AA2024-T351 in full immersion: a galvanic throwing power investigation using a scanning vibrating electrode technique. *J. Electrochem. Soc.* 165, C27–C41. doi: 10.1149/2.0711802jes
- Kannan, B., King, A. D., and Scully, J. R. (2015). Effect of pretreatments on Alloy 2024-T351 corrosion protection by magnesium-rich. Nonchromium primer (MgRP): laboratory characterization in full immersion. *Corrosion* 71, 1093–1109. doi: 10.5006/1700
- Kannan, B., and Scully, J. R. (2016). Performance of a magnesium-rich primer on pretreated AA2024-T351 in selected laboratory and field environments: Conversion coating pretreatments. *Corrosion* 72, 1363–1384. doi: 10.5006/2187
- Kannan, B., Wolanski, D. M., and Scully, J. R. (2018a). Performance of a magnesium-rich primer on pretreated AA2024-T351 in selected laboratory and field environments : anodization pretreatment. *Corrosion* 74, 654–668. doi: 10.5006/2424
- Kendig, M., and Scully, J. R. (1990). Basic aspects of electrochemical impedance application for the life prediction of organic coatings on metals. *Corrosion* 46, 22–29. doi: 10.5006/1.3585061
- King, A. D., Birbilis, N., and Scully, J. R. (2014b). Accurate electrochemical measurement of magnesium corrosion rates; A combined impedance mass-loss and hydrogen collection study. *Electrochim. Acta* 121, 394–406. doi: 10.1016/j.electacta.2013.12.124
- King, A. D., Kannan, B., and Scully, J. R. (2014a). Environmental degradation of a mg-rich primer in selected field and laboratory environments: part 1-without a topcoat. *Corrosion* 70, 512–535. doi: 10.5006/0988

- King, A. D., Lee, J. S., and Scully, J. R. (2015). Galvanic couple current and potential 892 distribution between a Mg electrode and 2024-T351 under droplets analyzed by 893 microelectrode arrays. *J. Electrochem. Soc.* 162, 12–23. doi: 10.1149/2.0121501jes
- King, A. D., Lee, J. S., and Scully, J. R. (2016). Finite element analysis of the galvanic couple current and potential distribution between Mg and 2024-T351 in a Mg rich primer configuration. *J. Electrochem. Soc.* 163, C342–C356. doi: 10.1149/2.0171607jes
- King, A. D., and Scully, J. R. (2011). Sacrificial anode-based galvanic and barrier corrosion protection of 2024-T351 by a Mg-rich primer and development of test methods for remaining life assessment. *Corrosion* 67, 1–22. doi: 10.5006/1.3590330
- Knudsen, O. Ø., Steinsmo, U., and Bjordal, M. (2005). Zinc-rich primers - Test performance and electrochemical properties. *Prog. Org. Coatings*, 54, 224–229. doi: 10.1016/j.porgcoat.2005.06.009
- Knudsen, O. Ø., Steinsmo, U., Bjordal, M., and Nijjer, S. (2001). Accelerated testing: correlation between four accelerated tests and five tears of offshore field testing. *JPCL* 18, 52–56.
- Koch, G. (2017). “Cost of corrosion,” in *Trends Oil Gas Corros. Res. Technol. Prod. Transm.*, ed. A. M. El-Sherik (Cambridge: Woodhead Publishing), 3–30.
- Koul, M. G., Sheetz, A., Ault, P., Repp, J., and Whitfield, A. (2014). The effect of Zn-rich coatings on the corrosion and cracking resistance of high strength armor steel. *Corrosion* 70, 337–350. doi: 10.5006/1027
- Koulombi, N., Tsangaris, G. M., Vourvahi, C., and Molnar, F. (1997). Corrosion resistance and dielectric properties of an iron oxide filled epoxy coating. *J. Coatings Technol.* 69, 53–59. doi: 10.1007/BF02696252
- Krieg, R., Rohwerder, M., Evers, S., Schuhmacher, B., and Schauer-Pass, J. (2012). Cathodic self-healing at cut-edges: The effect of Zn²⁺ and Mg²⁺ ions. *Corros. Sci.* 65, 119–127. doi: 10.1016/j.corsci.2012.08.008
- Lasaga, A. C. (2014). *Kinetic Theory in the Earth Sciences, Ch. 7*. Princeton, NJ: Princeton University Press.
- Leidheiser, H. R. (1982). Corrosion of painted metals — a review. *Corrosion* 38, 374–383. doi: 10.5006/1.3581899
- Leng, A., Streckel, H., and Stratmann, M. (1998). The delamination of polymeric coatings from steel. Part 1: calibration of the Kelvin probe and basic delamination mechanism. *Corros. Sci.* 41, 547–578. doi: 10.1016/S0010-938X(98)00166-8
- Lillard, R. S., Kruger, J., Tait, W. S., and Moran, P. J. (1994). Using local electrochemical impedance spectroscopy to examine coating failure. *Corrosion* 51, 251–259. doi: 10.5006/1.3294331
- Liu, C., Yang, V. A., and Kelly, R. G. (2019). Inhibition of cathodic kinetics by Zn²⁺ and Mg²⁺ on AA7050-T7451. *J. Electrochem. Soc.* 166, C134–C146. doi: 10.1149/2.0551906jes
- Maier, B., and Frankel, G. S. (2011). Behavior of magnesium-rich primers on AA2024-T3. *Corrosion* 67, 1–15. doi: 10.5006/1.3586018
- Mansfeld, F. (1990). Electrochemical impedance spectroscopy (EIS) as a new tool for investigating methods of corrosion protection. *Electrochim. Acta* 35, 1533–1544. doi: 10.1016/0013-4686(90)80007-B
- Mansfeld, F., Kendig, M. W., and Tsai, S. (1982). Evaluation of corrosion behavior of coated metals with ac impedance measurements. *Corrosion* 38, 478–485. doi: 10.5006/1.3577363
- Mansfeld, F., and Tsai, C. H. (1991). Determination of coating deterioration with EIS. I. Basic relationships. *Corrosion* 47, 958–963. doi: 10.5006/1.3585209
- Marchebois, H., Joiret, S., Savall, C., Bernard, J., and Touzain, S. (2002). Characterization of zinc-rich powder coatings by EIS and Raman spectroscopy. *Surf. Coatings Technol.* 157, 151–161. doi: 10.1016/S0257-8972(02)00147-0
- Marques, A. G., and Simões, A. M. (2014). EIS and SVET assessment of corrosion resistance of thin Zn-55% Al-rich primers: Effect of immersion and of controlled deformation. *Electrochim. Acta* 148, 153–163. doi: 10.1016/j.electacta.2014.10.015
- Marsh, J., Scantlebury, J. D., and Lyon, S. B. (2001). The effect of surface/primer treatments on the performance of alkyd coated steel. *Corros. Sci.* 43, 829–852. doi: 10.1016/S0010-938X(00)00070-6
- McMahon, M. E., Burns, J. T., and Scully, J. R. (2019a). New criteria for substrate protection against stress corrosion cracking in Al-Mg alloys based on non-polarizability of Zn-rich primers. *Prog. Org. Coatings*, 135, 392–409. doi: 10.1016/j.porgcoat.2019.05.049
- McMahon, M. E., Santucci, R. J. Jr., and Scully, J. R. (2019b). Advanced chemical stability diagrams to predict the formation of complex zinc compounds in chloride environment. *RSC Adv.* 9, 19905–19916. doi: 10.1039/C9RA00228F
- McMahon, M. E., Scully, J. R., and Burns, J. T. (2019c). Mitigation of intergranular cracking in Al-Mg alloys via Zn-based electrode potential control in sodium chloride solution. *Corrosion*, 75, 911–928. doi: 10.5006/3185
- Merten, B. J. E., Battocchi, D., and Bierwagen, G. P. (2015). Aluminum alloy 2024-T3 protection by magnesium-rich primer with chromate-free metal salts. *Prog. Org. Coatings*, 78, 446–454. doi: 10.1016/j.porgcoat.2014.09.013
- Moggridge, G. D., Lape, N. K., Yang, C., and Cussler, E. L. (2003). Barrier films using flakes and reactive additives. *Prog. Org. Coatings*, 46, 231–240. doi: 10.1016/S0300-9440(02)00180-7
- Montemor, M. F. (2014). Functional and smart coatings for corrosion protection : a review of recent advances. *Surf. Coat. Technol.* 258, 17–37. doi: 10.1016/j.surfcoat.2014.06.031
- Nanna, M. E., and Bierwagen, G. P. (2004). Mg-rich coatings: A new paradigm for Cr-free corrosion protection of Al aerospace alloys. *J. Coatings Technol. Res.* 1, 69–80. doi: 10.1007/s11998-004-0001-7
- Nazarov, A., Le Bozec, N., and Thierry, D. (2018). Scanning Kelvin Probe assessment of steel corrosion protection by marine paints containing Zn-rich primer. *Prog. Org. Coatings*, 125, 61–72. doi: 10.1016/j.porgcoat.2018.08.024
- Oblonsky, L. J. (2006). Surface-enhanced raman scattering from pyridine adsorbed on thin layers of stainless steel. *J. Electrochem. Soc.* 141:3312. doi: 10.1149/1.2059332
- Ogle, K. (2004). The alkaline stability of phosphate coatings I : ICP atomic emission spectroelectrochemistry. *Corros. Sci.* 46, 979–995. doi: 10.1016/S0010-938X(03)00182-3
- Ogle, K., Baudu, V., Garrigues, L., and Philippe, X. (2000). Localized electrochemical methods applied to cut edge corrosion. *J. Electrochem. Soc.* 147:3654. doi: 10.1149/1.1393954
- Orazem, M. E., and Tribollet, B. (2008). An integrated approach to electrochemical impedance spectroscopy. *Electrochim. Acta* 53, 7360–7366. doi: 10.1016/j.electacta.2007.10.075
- Orazem, M. E., and Tribollet, B. (2017). *Electrochemical Impedance Spectroscopy, 2nd editon*. Hoboken, NJ: Wiley.
- Paliwoda-Porebska, G., Stratmann, M., Rohwerder, M., Potje-Kamloth, K., Lu, Y., Pich, A. Z., et al. (2005). On the development of polypyrrole coatings with self-healing properties for iron corrosion protection. *Corros. Sci.* 47, 3216–3233. doi: 10.1016/j.corsci.2005.05.057
- Park, J. H., Yun, T. H., Kim, K. Y., Song, Y. K., and Park, J. M. (2012). The improvement of anticorrosion properties of zinc-rich organic coating by incorporating surface-modified zinc particle. *Prog. Org. Coatings*, 74, 25–35. doi: 10.1016/j.porgcoat.2011.09.012
- Parker, M., Shrivastava, S., and Kelly, R. G. (2015). Developing a framework for accelerated test design by investigating the impact of key testing variables on the exfoliation corrosion of AA2060. *ECS Meet. Abstr.* 14, 694–694.
- Pathak, S. S., Blanton, M. D., Mendon, S. K., and Rawlins, J. W. (2010). Investigation on dual corrosion performance of magnesium-rich primer for aluminum alloys under salt spray test (ASTM B117) and natural exposure. *Corros. Sci.* 52, 1453–1463. doi: 10.1016/j.corsci.2009.11.032
- Pathak, S. S., Mendon, S. K., Blanton, M. D., and Rawlins, J. W. (2012). Magnesium-based sacrificial anode cathodic protection coatings (Mg-Rich Primers) for aluminum alloys. *Metals* 2, 353–376. doi: 10.3390/met2030353
- Pereira, D., Scantlebury, J. D., Ferreira, M. G. S., and Almeida, M. E. (1990). The application of electrochemical measurements to the study and behaviour of zinc-rich coatings. *Corros. Sci.* 30, 1135–1147. doi: 10.1016/0010-938X(90)90061-9
- Petry, L., and Hansen, D. C. (2016). A comparative study of two coating systems exposed for 2 years in the field and in accelerated atmospheric corrosion chamber environments. *Corrosion* 72, 1385–1396. doi: 10.5006/2084
- Place, B. J. (2019). Activity analysis of iron in water using a simple LED spectrophotometer. *J. Chem. Educ.* 96, 714–719. doi: 10.1021/acs.jchemed.8b00515

- Plagemann, P., Weise, J., and Zockoll, A. (2013). Zinc-magnesium-pigment rich coatings for corrosion protection of aluminum alloys. *Prog. Org. Coatings* 76, 616–625. doi: 10.1016/j.porgcoat.2012.12.001
- Presuel-Moreno, F., Jakab, M. A., Tailleart, N., Goldman, M., and Scully, J. R. (2008). Corrosion-resistant metallic coatings. *Mater. Today* 11, 14–23. doi: 10.1016/S1369-7021(08)70203-7
- Presuel-Moreno, F. J., Goldman, M. E., Kelly, R. G., and Scully, J. R. (2005b). Electrochemical sacrificial cathodic prevention provided by an Al-Co-Ce metal coating coupled to AA2024-T3. *J. Electrochem. Soc.* 152, B302–B310. doi: 10.1149/1.1943588
- Presuel-Moreno, F. J., Jakab, M. A., and Scully, J. R. (2005a). Inhibition of the oxygen reduction reaction on copper with cobalt, cerium, and molybdate ions. *J. Electrochem. Soc.* 152, B376–B387. doi: 10.1149/1.1997165
- Presuel-Moreno, F. J., Wang, H., Jakab, M. A., Kelly, R. G., and Scully, J. R. (2006). Computational modeling of active corrosion inhibitor release from an Al-Co-Ce metallic coating protection of exposed AA2024-T3. *J. Electrochem. Soc.* 153, B486–B498. doi: 10.1149/1.2335946
- Prosek, T., Nazarov, A., Bexell, U., Thierry, D., and Serak, J. (2008). Corrosion mechanism of model zinc-magnesium alloys in atmospheric conditions. *Corros. Sci.* 50, 2216–2231. doi: 10.1016/j.corsci.2008.06.008
- Rafla, V. N., Khullar, P., Kelly, R. G., and Scully, J. R. (2018). Coupled multi-electrode array with a sintered Ag/AgCl counter/reference electrode to investigate AA7050-T7451 and Type 316 stainless steel galvanic couple under atmospheric conditions. *J. Electrochem. Soc.* 165, C562–C572. doi: 10.1149/2.1001809jes
- Rafla, V. N., and Scully, J. R. (2019). Galvanic couple behavior between AA7050-T7451 and stainless steel in a fastener arrangement assessed with coupled multi-electrode arrays under atmospheric exposure conditions. *Corrosion* 75, 12–28. doi: 10.5006/2885
- Rebhan, M., Rohwerder, M., and Stratmann, M. (2003). Delamination of polymeric coatings on silidized iron. *Mater. Corros.* 54, 19–22. doi: 10.1002/maco.200390001
- Rohwerder, M., Duc, L. M., and Michalik, A. (2009). *In situ* investigation of corrosion localised at the buried interface between metal and conducting polymer based composite coatings. *Electrochim. Acta* 54, 6075–6081. doi: 10.1016/j.electacta.2009.02.103
- Rohwerder, M., Isik-Uppenkamp, S., and Amarnath, C. A. (2011). Application of the Kelvin Probe method for screening the interfacial reactivity of conducting polymer based coatings for corrosion protection. *Electrochim. Acta* 56, 1889–1893. doi: 10.1016/j.electacta.2010.09.098
- Salgueiro Azevedo, M., Allely, C., Ogle, K., and Volovitch, P. (2015). Corrosion mechanisms of Zn(Mg,Al) coated steel: 2. The effect of Mg and Al alloying on the formation and properties of corrosion products in different electrolytes. *Corros. Sci.* 90, 482–490. doi: 10.1016/j.corsci.2014.07.042
- Santucci, R. J., Kannan, B., Abbott, W., and Scully, J. (2018b). Scientific investigation of the corrosion performance of magnesium and magnesium oxide primers on Al Alloy 2024-T351 in field exposures. *Corrosion* 75, 440–456. doi: 10.5006/2879
- Santucci, R. J., Kannan, B., Abbott, W., and Scully, J. R. (2017a). Magnesium and magnesium oxide primer on AA2024-T351: assessment of field performance. *Corrosion* 73, 1196–1201. doi: 10.5006/2545
- Santucci, R. J., McMahon, M. E., and Scully, J. R. (2018a). Utilization of chemical stability diagrams for improved understanding of electrochemical systems: evolution of solution chemistry towards equilibrium. *Npj Mater. Degrad.* 2, 1–9. doi: 10.1038/s41529-017-0021-2
- Santucci, R. J., Kannan, B., and Scully, J. R. (2017b). Electrochemical diagnostic cycle testing on magnesium and magnesium oxide-pigmented primers on 2024-T351. *Corrosion* 74, 96–111. doi: 10.5006/2547
- Schaefer, K., and Miszczyk, A. (2013). Improvement of electrochemical action of zinc-rich paints by addition of nanoparticulate zinc. *Corros. Sci.* 66, 380–391. doi: 10.1016/j.corsci.2012.10.004
- Scully, J. R., and Jakab, M. A. (2006). Design of cathodic inhibitors for AA2024-T3 guided by understanding heterogeneous cathodic reaction kinetics. *ECS Trans.* 1, 47–63. doi: 10.1149/1.2215578
- Shreepathi, S., Bajaj, P., and Mallik, B. P. (2010). Electrochemical impedance spectroscopy investigations of epoxy zinc rich coatings: Role of Zn content on corrosion protection mechanism. *Electrochim. Acta* 55, 5129–5134. doi: 10.1016/j.electacta.2010.04.018
- Shtoyko, T., Stuart, O. D., and Gray, H. N. (2007). Spectroelectrochemical sensing of aqueous iron : an experiment for analytical chemistry. *J. Chem. Educ.* 84, 1467–1470. doi: 10.1021/ed084p1467
- Simoes, A., Battocchi, D., Tallman, D., and Bierwagen, G. (2008). Assessment of the corrosion protection of aluminium substrates by a Mg-rich primer : EIS, SVET and SECM study. *Prog. Org. Coatings* 63, 260–266. doi: 10.1016/j.porgcoat.2008.02.007
- Sinko, J. (2001). Challenges of chromate inhibitor pigments replacement in organic coatings. *Prog. Org. Coatings* 42, 267–282. doi: 10.1016/S0300-9440(01)00202-8
- Sørensen, P. A., Kiil, S., Dam-Johansen, K., and Weinell, C. E. (2009). Anticorrosive coatings : a review. *J. Coatings Technol. Res.* 6, 135–176. doi: 10.1007/s11998-008-9144-2
- Stouil, J., Prosek, T., Nazarov, A., Oswald, J., Kriz, P., and Thierry, D. (2015). Electrochemical properties of corrosion products formed on Zn-Mg, Zn-Al and Zn-Al-Mg coatings in model atmospheric conditions. *Mater. Corros.* 66, 777–782. doi: 10.1002/maco.201408058
- Stratmann, M., Feser, R., and Leng, A. (1994). Corrosion protection by organic films. *Electrochim. Acta* 39, 1207–1214. doi: 10.1016/0013-4686(94)E0038-2
- Taylor, M. L., Blanton, M., Konecki, C., Rawlins, J., and Scully, J. R. (2015a). Scribe creep and underpaint corrosion on ultra high molecular weight epoxy resin coated 1018 steel (UNS G10180) Part I : comparison of field exposures to standard lab accelerated life tests. *Corrosion* 71, 71–91. doi: 10.5006/1348
- Taylor, M. L., Blanton, M., Konecki, C., Rawlins, J., and Scully, J. R. (2015b). Scribe creep and underpaint corrosion on ultra-high molecular weight epoxy resin coated 1018 steel part 2: scribe creep model as a function of environmental severity factors. *Corrosion* 71, 326–342. doi: 10.5006/1349
- Thomas, N. L. (1991). The barrier properties of paint coatings. *Prog. Org. Coatings* 19, 101–121. doi: 10.1016/0033-0655(91)80001-Y
- Thomas, S., Birbilis, N., Venkatraman, M. S., and Cole, I. S. (2013). Self-repairing oxides to protect zinc: review. Discussion and prospects. *Corros. Sci.* 69, 11–22. doi: 10.1016/j.corsci.2013.01.011
- Tran, T. T. M., Tribollet, B., and Sutter, E. M. M. (2016). New insights into the cathodic dissolution of aluminium using electrochemical methods. *Electrochim. Acta* 216, 58–67. doi: 10.1016/j.electacta.2016.09.011
- Tsai, C. H., and Mansfeld, F. (1993). Determination of coating deterioration with EIS: Part II. Development of a method for field testing of protective coatings. *Corrosion* 49, 726–737. doi: 10.5006/1.3316106
- Upadhyay, V., and Battocchi, D. (2016). Localized electrochemical characterization of organic coatings : a brief review. *Prog. Org. Coatings* 99, 365–377. doi: 10.1016/j.porgcoat.2016.06.012
- Vakili, H., Ramezanzadeh, B., and Amini, R. (2015). The corrosion performance and adhesion properties of the epoxy coating applied on the steel substrates treated by cerium-based conversion coatings. *Corros. Sci.* 94, 466–475. doi: 10.1016/j.corsci.2015.02.028
- Vilche, J. R., Bucharsky, E. C., and Giudice, C. A. (2002). Application of EIS and SEM to evaluate the influence of pigment shape and content in ZRP formulations on the corrosion prevention of naval steel. *Corros. Sci.* 44, 1287–1309. doi: 10.1016/S0010-938X(01)00144-5
- Volovitch, P., Allely, C., and Ogle, K. (2009). Understanding corrosion via corrosion product characterization: I. Case study of the role of Mg alloying in Zn-Mg coating on steel. *Corros. Sci.* 51, 1251–1262. doi: 10.1016/j.corsci.2009.03.005
- Volovitch, P., Vu, T. N., Allély, C., Abdel Aal, A., and Ogle, K. (2011). Understanding corrosion via corrosion product characterization: II. Role of alloying elements in improving the corrosion resistance of Zn-Al-Mg coatings on steel. *Corros. Sci.* 53, 2437–2445. doi: 10.1016/j.corsci.2011.03.016
- Walter, G. W. (1986). A critical review of the protection of metals by paints. *Corros. Sci.* 26, 27–38. doi: 10.1016/0010-938X(86)90120-4
- Wang, H., Presuel, F., and Kelly, R. G. (2004). Computational modeling of inhibitor release and transport from multifunctional organic coatings. *Electrochim. Acta* 49, 239–255. doi: 10.1016/j.electacta.2003.08.006
- Wang, J., Zuo, Y., and Tang, Y. (2013). The study on Mg-Al rich epoxy primer for protection of aluminum alloy. *Int. J. Electrochem. Sci.* 8, 10190–10203.

- Wang, Q. (2012). *The Role of Zinc Particle Size and Loading in Cathodic Protection Efficiency*. Richmond, VA: Virginia Commonwealth University.
- Williams, G., Birbilis, N., and McMurray, H. N. (2015). Controlling factors in localised corrosion morphologies observed for magnesium immersed in chloride containing electrolyte. *Faraday Discuss.* 180, 313–330. doi: 10.1039/C4FD00268G
- Williams, G., Coleman, A. J., and McMurray, H. N. (2010). Inhibition of Aluminium Alloy AA2024-T3 pitting corrosion by copper complexing compounds. *Electrochim. Acta* 55, 5947–5958. doi: 10.1016/j.electacta.2010.05.049
- Williams, G., Dafydd, H., and Grace, R. (2013). The localised corrosion of Mg alloy AZ31 in chloride containing electrolyte studied by a scanning vibrating electrode technique. *Electrochim. Acta* 109, 489–501. doi: 10.1016/j.electacta.2013.07.134
- Williams, G., Dafydd, H., and Subramanian, R. (2014). Chloride ion concentration effects on passivity breakdown in magnesium. *ECS Trans.* 58, 23–34. doi: 10.1149/05831.0023ecst
- Williams, G., Geary, S., and McMurray, H. N. (2012). Smart release corrosion inhibitor pigments based on organic ion-exchange resins. *Corros. Sci.* 57, 139–147. doi: 10.1016/j.corsci.2011.12.024
- Williams, G., and McMurray, H. N. (2001). Chromate inhibition of corrosion-driven organic coating delamination studied using a scanning kelvin probe technique. *J. Electrochem. Soc.* 148, B337–B385. doi: 10.1149/1.1396336
- Williams, G., McMurray, H. N., and Worsley, D. A. (2002). Cerium (III) inhibition of corrosion-driven organic coating delamination studied using a scanning kelvin probe technique. *J. Electrochem. Soc.* 149, B154–B162. doi: 10.1149/1.1457983
- Xavier, J. R., and Nishimura, T. (2017). Evaluation of the corrosion protection performance of epoxy coatings containing Mg nanoparticle on carbon steel in 0.1 M NaCl solution by SECM and EIS techniques. *J. Coatings Technol. Res.* 14, 395–406. doi: 10.1007/s11998-016-9856-7
- Xia, L., Akiyama, E., Frankel, G., and McCreery, R. (2000). Storage and release of soluble hexavalent chromium from chromate conversion coatings equilibrium aspects of Cr^{VI} concentration. *J. Electrochem. Soc.* 147, 2556–2562. doi: 10.1149/1.1393568
- Yan, M., Gelling, V. J., Hinderliter, B. R., Battocchi, D., Tallman, D. E., and Bierwagen, G. P. (2010). SVET method for characterizing anti-corrosion performance of metal-rich coatings. *Corros. Sci.* 52, 2636–2642. doi: 10.1016/j.corsci.2010.04.012
- Yang, C., Smyrl, W. H., and Cussler, E. L. (2004). Flake alignment in composite coatings. *J. Memb. Sci.* 231, 1–12. doi: 10.1016/j.memsci.2003.09.022
- Yasakau, K. A., Zheludkevich, M. L., Lamaka, V. S., and Ferreira, M. G. S. (2006). Mechanism of corrosion inhibition of AA2024 by rare-earth compounds. *J. Phys. Chem. B.* 110, 5515–5528. doi: 10.1021/jp0560664
- Zhang, L., Ma, A., Jiang, J., Song, D., Chen, J., and Yang, D. (2012). Anti-corrosion performance of waterborne Zn-rich coating with modified silicon-based vehicle and lamellar Zn (Al) pigments. *Prog. Nat. Sci. Mater. Int.* 22, 326–333. doi: 10.1016/j.pnsc.2012.07.001
- Zheludkevich, M. L., Tedim, J., and Ferreira, M. G. S. (2012). “Smart” coatings for active corrosion protection based on multi-functional micro and nanocontainers. *Electrochim. Acta.* 82, 314–323. doi: 10.1016/j.electacta.2012.04.095
- Zhu, Y., Sun, K., and Frankel, G. S. (2018). Intermetallic phases in aluminum alloys and their roles in localized corrosion. *J. Electrochem. Soc.* 165, C807–C820. doi: 10.1149/2.0931811jes
- Zou, S., Williams, C. T., Chen, E. K.-Y., and Weaver, M. J. (1998). Surface-enhanced raman scattering as a ubiquitous vibrational probe of transition metal interfaces: benzene and related chemisorbates on palladium and rhodium in aqueous solution. *J. Phys. Chem. B* 102, 9039–9049. doi: 10.1021/jp9824205

Conflict of Interest Statement: The authors declare that the research was conducted in the absence of any commercial or financial relationships that could be construed as a potential conflict of interest.

Copyright © 2019 McMahon, Santucci, Glover, Kannan, Walsh and Scully. This is an open-access article distributed under the terms of the Creative Commons Attribution License (CC BY). The use, distribution or reproduction in other forums is permitted, provided the original author(s) and the copyright owner(s) are credited and that the original publication in this journal is cited, in accordance with accepted academic practice. No use, distribution or reproduction is permitted which does not comply with these terms.